Ferhan Öztürk

FINITE ELEMENT MODELLING OF TUBULAR BOLTED CONNECTION OF A LATTICE WIND TOWER FOR FATIGUE ASSESSMENT

FCTUC
2016

FCTUC **DEPARTAMENTO DE ENGENHARIA CIVIL**
FACULDADE DE CIÊNCIAS E TECNOLOGIA
UNIVERSIDADE DE COIMBRA

isise Institute for Sustainability and Innovation in Structural Engineering

FINITE ELEMENT MODELLING OF TUBULAR BOLTED CONNECTION OF A LATTICE WIND TOWER FOR FATIGUE ASSESSMENT

Ferhan Öztürk

Supervisors: Professor Carlos Rebelo
Dr. José Correia

European Commission
ERASMUS MUNDUS

Thesis Submitted in partial fulfillment of requirements for the degree of Master of Science in Construction of Steel and Composite Structures
European Erasmus Mundus Master
Sustainable Constructions under natural hazards and catastrophic events

University of Coimbra
05.02.2016

FINITE ELEMENT MODELLING OF TUBULAR BOLTED CONNECTION OF A LATTICE WIND TOWER FOR FATIGUE ASSESSMENT

Author: Ferhan Öztürk

Supervisors: Professor Carlos Rebelo
Dr. José Correia

University: University of Coimbra

University: University of Coimbra

Date: 05.02.2016

ACKNOWLEDGEMENT

I would like to give my special thanks to professor Carlos Rebelo and doctor José António Correia for their valuabe input and constructive comments in this thesis.

Secondly, I owe a debt of gratitute to the greatest man of past century, Mustafa Kemal Atatürk whose light still shines upon our path to see the importance of science and purpose of being a human. I also would like to express my gratitude to professor Oktay Sinanoğlu whose books taught me the formula of "Science+Heart" to become a true scientist.

Last but not the least, I heartfully thank to my friends, family and loved ones which constitude the most important part of my life.

ABSTRACT

One of the biggest challenges in front of the growing wind energy industry is to build higher towers for wind energy converters. In order to deal with such a problem a new hybrid tower, comprising a steel lattice lower part and a steel tubular upper part solution was proposed. The solution is targeted at tall onshore applications which are more effective in energy generation in situations where wind shear profile is clearly benefiting higher turbines, for example near forests. As part of this project, this thesis is focused on the fatigue assessment of tubular bolted connection of lattice tower.

In first chapter, commercial towers for wind energy converters are briefly introduced, namely, concrete towers, welded steel shell towers, concrete/steel hybrid towers, lattice towers and hybrid lattice-tubular towers.

In the second chapter, developments in fatigue analysis during the last decades and fatigue life prediction methods are given. Moreover, special emphasis is given to multiaxial fatigue life criteria which was used in fatigue life calculation of the connection used in this thesis.

In the third chapter, numerical finite element modelling steps for stiffness calculation, global beam element model, and local connection model are given in detail. Additionally, finite element stress-strain results and fatigue life calculations using these results are also explained.

In the last chapter, conclusions are drawn and further possible improvements of this work is suggested.

KEY WORDS

Lattice tower, tubular bolted connection, finite element analysis, multiaxial fatigue criteria, fatigue assessment

TABLE OF CONTENTS

FIGURE INDEX

TABLE INDEX

NOTATIONS

LATIN

a	Crack length
b	Fatigue strength exponent
c	Fatigue ductility exponent
da/dN	Fatigue crack growth rate
D	Total damage
E	Modulus of elasticity
f_y	Higher yield stress
f_u	Ultimate tensile strength
H(x)	Heaviside function
$J_{2,a}$	Amplitude of second invariant of deviatoric stress tensor
K	Stress intensity factor
K’	Cyclic strength coefficient
K_f	Fatigue notch factor
K_t	Total tress concentration factor
n	Strain hardening exponent
n’	Cyclic strain-hardening exponent
N	Number of cycles (fatigue life)
N_f	Number of cycles to failure
N_i	Number of cycles in crack initiation; Number of cycles of the specimen i
N_T	Total number of cycles
$2N_f$	Reversals to failure
$2N_t$	Transition Number of reversals
R	Stress ratio
S_k	Material dependant constant
SWT	Smith, Watson and Topper fatigue damage parameter
ΔK_{eq}	Equivalent stress intensity range
ΔK_I	Range of stress intensity factor
ΔW	Total strain energy range

ΔW^{E+} Elastic strain energy range associated with the tensile stress

ΔW^{P} Plastic strain energy density

ΔW^{t} Elastic tensile strain energy density

GREEK

$\sigma_{H,max}$ Maximum value of the hydrostatic stress

τ_a Alternating shear stress

γ_{max} Maximum shear strain

ε_1 First principal strain

ε_3 Third principal strains

θ_1 Indicator of loading a cycle

θ_2 Indicator of unloading of a cycle

σ_n^{max} Maximum normal stress

$\bar{\nu}$ Poisson's ratio

$\Delta\gamma$ Range of shear strain

$\Delta\tau$ Range of shear stress

$\Delta\varepsilon_n$ Normal strain range

$\Delta\sigma_n$ Normal stress range

$\bar{\rho}$ Multiaxial constraint ratio

ACRONYMS

DIC Digital Image Correlation

EC3 Eurocode 3

FS Fatemi-Socie

JV Jahed-Varvani

KBM Kandil, Brown and Miller

SWT Smith, Watson and Topper

1. INTRODUCTION

The utilisation of wind energy is not a new technology but draws on the rediscovery of a long tradition of wind power technology. It is no longer possible now to tell from the remainders of historical "wind power plants" just how important a role wind power played in the past. The triumphal spread of the cheap coal and oil fuels and of easy energy distribution in the form of electricity was so complete that the losers, windmills and wind wheels, could only survive in economic niches of little importance. Today, while energy production based on the burning of coal and oil or on the splitting of the uranium atom is meeting with increasing resistance, regardless of the various reasons, the re-emergence of wind power is an almost inevitable consequence. In today's world alternative energy resources are becoming increasingly more important considering the limited fossil fuel resources and the wild competition to obtain them [1].

The process of commercialising and monopolisation of wind turbines has driven governments and big companies to build bigger wind turbines which also helps other sectors to increase their productions. However, even though having the technology to build bigger parts or segments of towers is not enough to overcome some other problems to build towers, such as transportation and lifting. Consequently, using smaller parts that can be assembled on site to build towers such as lattice towers was considered to be an option to avoid such problems. To have an opportunity to build higher lattice towers seems to be a good solution, yet the need to improve any invention persists. As well as the invention of different lattice towers, some inherent weaknesses of any structure like fatigue is still of a concern for such inventions.

1.1 Motivation

The need for obtaining higher and stable wind flow to generate more electricity requires higher wind towers. As one of the most cost effective solutions among all is lattice towers, this study is focused on assessing an important aspect, fatigue life, of a newly proposed bolted connection of tubular cross section of an octagonal lattice tower.

1.2 Objectives

Recently, a steel hybrid solution for onshore wind turbine towers using a lattice structure for the lower portion of the tower and a tubular upper portion was proposed. This solution targeted tall onshore applications supporting multi megawatt wind turbines. Previous developments focused on conceptual design and structural predesign of one case study based on equivalent load tables and using S355 steel grade: hub height 150 meters (40 meters lattice part, 110 meters tubular part) supporting a 5 MW wind turbine. The aim of this thesis can be divided into three main categories. First, to develop a finite element (FE) model of a steel half-pipes bolted connection for stiffness assessment, second application of obtained stiffness of the bolted joint to a global beam element model to obtain a more realistic member forces compared to a pinned connection and for the last step, to apply member forces obtained in the global analysis to local FE model in order to obtain stresses and strains to be used in a multiaxial fatigue assessment with a local approach.

1.3 Organisation of the Thesis

The thesis begins with an introduction in which the motivation, objectives and structure of the thesis and brief information about types of towers used for wind energy converters are presented.

The introduction is followed by a literature review on fatigue that is composed of the following topics: a historic perspective on fatigue, stages of fatigue damage, and review of the main factors influencing fatigue damage, distinct approaches to fatigue modelling including global *S-N* approaches, local approaches and Fracture Mechanics based approaches.

In third chapter, numerical modelling details of tubular bolted connection of the lattice tower which includes stiffness calculation of the joint, general beam analysis of the lattice tower and local connection model and results are presented.

In the fourth and the final chapter, conclusions are drawn and further possible improvements are suggested.

1.4 Towers Used for Wind Energy Converters

The use of wind energy to generate electricity is now well accepted with a large industry manufacturing and installing tens of GWs of new capacity each year. Although there are exciting new developments, particularly in very large wind turbines, and many challenges remain, there is a considerable body of established knowledge concerning the science and

technology of wind turbines. The overwhelming majority of wind turbines presently in use are horizontal axis connected to a large electricity network [2].

Supporting structures for wind turbines are often tubular structures made of traditional structural materials, namely, steel and concrete. There is also hybrid concrete/steel wind turbine towers in which combination of concrete and steel tubes are used in the lower and upper part respectively. Most commonly pre-fabricated concrete segments and steel tubes with maximum diameter of about 4 m are transported by the truck to the site. Increasing requirements in efficiency and competiveness of wind turbines in generation of electrical energy lead to larger swept area, meaning the longer rotor blades, and higher hub height. Such developments, towers higher than 100 m were favourable for development of steel lattice towers [2].

1.4.1 Type of Towers for Wind Energy Converters

A structural tower or some other support structure is needed to raise the nacelle assembly that could weigh several cubic tonnes up into the air, away from the slower and more turbulent winds near the ground. It elevates the rotor to a height where the wind velocity is significantly larger and less perturbed than near the ground level. Some towers can reach 135 m in height necessitating that their structures are capable of withstanding significant loads due to gravity, rotation and wind thrust loads [2].

The tower accounts for approximately 20% of the total manufacturing cost for a wind turbine [3]. For turbines with higher rated power capacity, the percentage could be even increasing. Reduction of cost could be made through various methods: optimization of structural form can save material cost if sufficient structural strength is maintained or manufacturing cost can be lowered by means of mass production. The latter is in fact the reason why large scale wind farm development is becoming the interests of many.

As for optimization of structural form, the 20% or even higher cost of the tower could be possibly reduced if for instance lattice structure is applied as support structure for wind turbine. Lattice structure possesses advantages in that it generally requires less material; the wave load impact in the offshore environment is also reduced due to the reduced impacted area compared with monopile structure. On the other hand, transportation of lattice structure is also much more convenient when road transportation capacity of 4-6m is limited if a larger dimension of monopile is required for a larger scale wind turbine.

1.4.1.1 Concrete Towers

In a concrete tower the concrete proper only withstands pressure. The ability to absorb tension is provided primarily by pretensioned tendons, located in ducts in the concrete or internal/external of the concrete walls. Making them internal or external enables easy inspection. There are also traditional untensioned reinforcement bars cast into the concrete shell, necessary to provide the compressive strength.

A concrete tower is clearly dimensioned by the extreme load case, since it has large margins towards fatigue. It is assumed that the concrete is pretensioned by the tendons to 20 MPa. In the extreme load case the pressure side is offloaded to close to zero whereas the tension on the other side is doubled. By increasing the thickness of the concrete cover it may be possible to increase the lifetime to e.g. 50 years. One concrete tower may then serve for two generations of machineries, with obvious economical savings (Figure 1). Compared to steel towers, concrete towers are much heavier and takes longer time to erect. On the other hand, the concrete or the concrete elements, if made small enough, are not subject to transportation restrictions, as for the case with welded steel towers with large base diameters.

Regardless if the tower is slip formed or assembled from precast elements, it is advantageous to install the post-stressing tendons from below, thus not needing to lift the heavy rolls of tendons to the tower top. Then it is however necessary to furnish the foundation with a cellar [2].

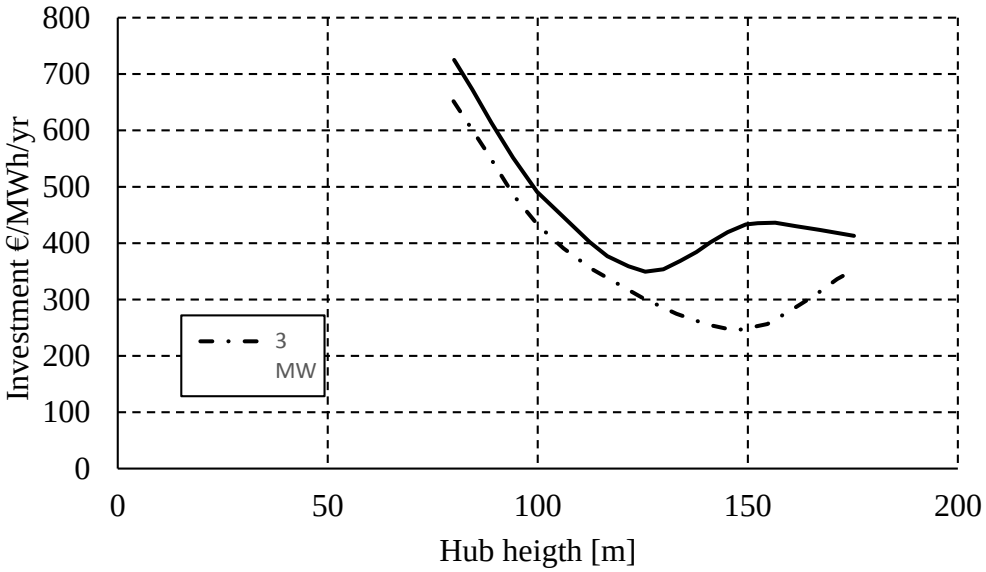

Figure 1. Summary of specific investment cost for 3 and 5 MW wind turbines furnished with slip formed concrete towers.

1.4.1.2 Welded Steel Shell Towers

The welded steel shell tower today dominates the wind turbine market. It consists of cylinders made of steel plate bent to a circular shape and welded longitudinally (Figure 2). Transversal welds connect several such cylinders to form a tower section. Each section ends with a steel flange in each end. The sections are bolted to each other. The bottom flange is connected to the foundation and the top one to the nacelle.

A tower is primarily dimensioned against tension and buckling in the extreme load cases. Ideally the margin should be the same for both criteria, since increasing the diameter, with a corresponding reduction of plate thickness, increases the tension strength but reduces the buckling margin. Finally the tower has to be checked against fatigue. According to BSK and Eurocode connecting welds (transversal and longitudinal) and dimension changes (flanges) affects the strength in a negative way. Thus it is the welds and the geometry that primarily determine the fatigue strength rather than the quality of the steel. Therefore wind turbine towers mostly use ordinary qualities of steel. In this report use of S355J2G3 (earlier known as SS2134, tensile yield limit 355 MPa) is assumed for both the welded and friction joint towers [2].

In the dimensioning load case, the tower is affected by the thrust from the rotor. This thrust will create a bending moment, which increases with the distance from the turbine shaft, i.e. inversely proportional to the height above the ground. To cope with this increasing bending moment it is favourable to make the tower conical in shape, to the limit of buckling. However, land transportation even with a special permit is not possible for diameters exceeding 4,5 m in many countries (Figure 3).

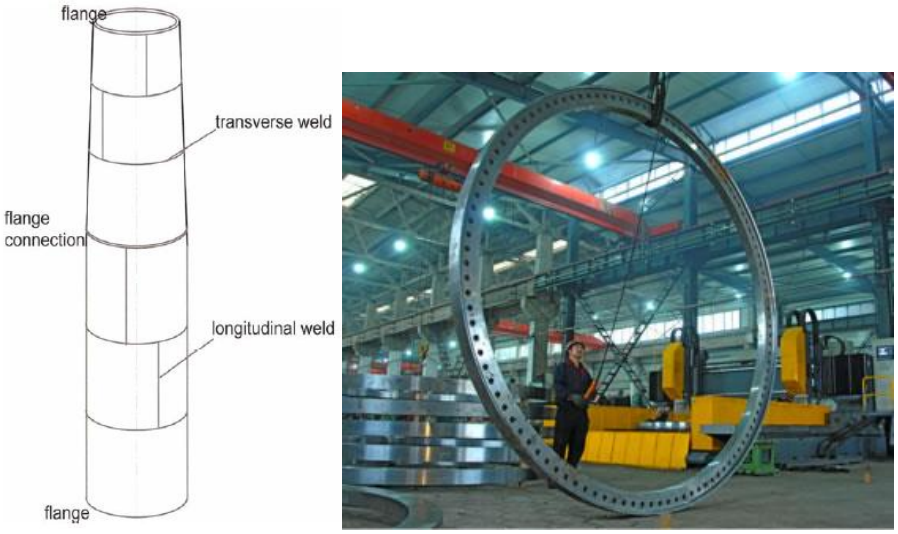

Figure 2. Steel shell tower in two sections and ring flange.

Ring flange connections result in high fabrication cost and long delivery times. Another disadvantage of such connections is their low fatigue resistance which is approximately 50 MPa.

Figure 3. Transportation of steel tubular tower segments.

1.4.1.3 Concrete/Steel Hybrid Tower

The idea behind building a hybrid concrete/steel tower (Figure 4) is to use concrete in the wide lower part and steel in the upper part, where a conventional welded steel shell tower section may be designed without any risk of conflict with the transportation limitations. In reality it also makes it easier to design the concrete part and to get the eigen-frequencies right [2].

Figure 4. Concrete-steel hybrid tower.

1.4.1.4 Lattice Tower

Lattice tower applied as wind turbine support structure does not come until recently. In fact, during the earliest period of onshore wind turbine development, lattice tower was already

adopted. This type of structure is simple to construct and stiff in function. A lot of such structures can be seen on the early onshore wind turbines (Figure 5).

As the size of wind turbine increased, lattice tower was gradually displaced by tubular tower. In the early experimental stage of wind energy and especially when the size of wind turbine was still moderate, the emphasis was not placed on cost reduction of the tower, which is why the tubular tower was very widely and popularly used. However, as commercialization of wind energy is urged and the size of wind turbine grows, after cost reduction measurements on mechanical components like the gearbox and generator are achieved, cost minimization associated with the turbine support structure is again attracting interests and this is why these years the lattice structure is receiving more and more attentions, especially on large scale offshore wind turbines [2].

Figure 5. Steel lattice tower.

The visual qualities are controversial, especially due to the resemblance to towers for high-voltage power lines, generally claimed to be ugly. An open design, like a lattice tower, is more prone to icing than a tubular tower. The possible impact on the dynamic properties may be the most severe consequence, which may endanger the wind turbine in an extreme case. It may also be a problem for maintenance personnel, even if their elevator runs on heated rails. Increased risk of falling ice is also another important danger for such towers.

1.4.1.5 Hybrid Lattice-Tubular Towers

Use of hybrid towers is possible to achieve greater heights for the turbine shaft. This type of towers is composed of 3 parts, the lower lattice part fixed to the foundation and assembled at the installation site, a piece of tubular tower consisting of several parts bolted together, as happens in most tubular towers, and a transition piece which ensures the connection and transmission of efforts between the two main parts.

A tower of this kind was installed at the wind farm in Gujarat, India some years ago (Figure 6). It is expected that this new type of towers produces about 10 to 12% more energy, because gains against the normal towers more than 40 meters in total height, with a combined height of 120 meters against the 80 meters of most tubular towers, therefore an ideal bet for low wind areas, due to its superior performance, with a potential to be installed in all parts of the world, without having to look for places where the wind speed is high. These towers can be climbed from the inside, and have platforms inside the tubular part for maintenance and repair work, but also to maintain all the equipment necessary for its operation.

Figure 6. Hybrid lattice-tubular tower.

Different types of towers for wind energy converters are given above. A cost comparison for currently existing tower types are also given in Figure 7 below [2].

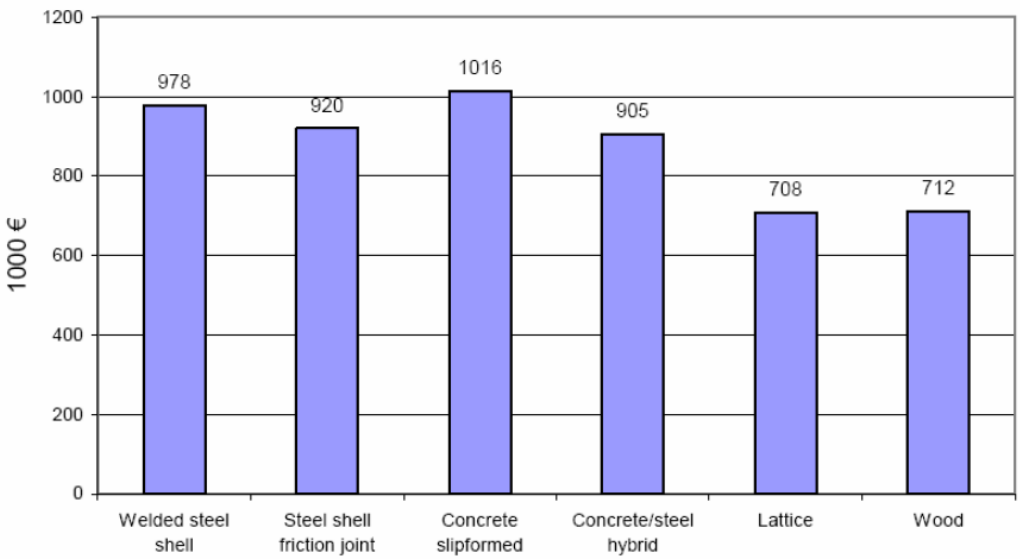

Figure 7. Tower costs for the alternative designs. Turbine power 3 MW, hub height 125 m.

2. State of the Art in Fatigue

2.1 History of Fatigue

Fatigue failures in metallic structures are a well-known phenomenon which has caused many injuries and much financial loss. On the other hand, compared to very large number of thriving mechanical structure and component design, mechanical failures are of little consequence. Fatigue was not noticed in 19th century because damage could not be seen before failures occurred unexpectedly. Later in 20th century, it has been experienced that repetitive loads can initiate a fatigue mechanism in the material leading to nucleation of a microcrack, crack growth and finally to a complete failure of structure. Such failures were first observed in 19th century and started to be investigated. One of the most important research work on fatigue has been carried out by August Wöhler. He realized that a relatively low force compared to static strength of the structure can cause failure if repeatedly applied. Using stress versus life diagrams (*S*-*N*), he showed with higher stress amplitudes fatigue life decreased and below a certain stress amplitude test specimens did not fail. He also realized that stress range is more important than maximum stress [3].

During the 1870s and 1890s additional researchers substantiated and expanded Wohler's classical work Gerber and others investigated the influence of mean stress, and Goodman proposed a simplified theory concerning mean stress. Their names are still associated with diagrams involving alternating and mean stresses. Bauschinger in 1886 showed that the yield strength in tension or compression was reduced after applying a load of the opposite sign that caused inelastic deformation. This was the first indication that a single reversal of inelastic strain could change the stress-strain behaviour of metals. It was the forerunner of understanding cyclic softening and hardening of metals.

In the early 1900s Ewing and Humfrey used the optical microscope to pursue the study of fatigue mechanisms. Localized slip and slip band leading to the formation of microcracks were observed. Basquin in 1910 showed that alternating stress versus number of cycles to failure(*S*-*N*) in the finite life region could be represented as a log-log linear relationship. His equation, plus modifications by others, are currently used to represent finite life fatigue behaviour. In the 1920s, Gough and associates contributed greatly to the understanding of fatigue mechanisms. They also showed the combined effects of bending and torsion (multiaxial fatigue). Gough published a comprehensive book on fatigue of metals in 1924. Mooree and Kommersf published the first comprehensive American book on fatigue of metals in 1927. In 1920 Griffiths published the results of his theoretical calculations and experiments on brittle fracture using glass. He found that the strength of glass depended on the size of microscopic cracks. With this classical pioneering work on the importance of cracks, Griffith developed the basis for fracture mechanics. He thus became the "early father" of fracture

mechanics. In 1924, Palmgren developed a linear cumulative damage model for variable amplitude loading and established the use of the B10 fatigue life based upon statistical scatter for ball bearing design. McAdam in the 1920s performed extensive corrosion fatigue studies in which he showed significant degradation of fatigue resistance in various water solutions. This degradation was more pronounced in higher-strength steels. In 1930 Haighh presented a rational explanation of the difference in the response of high tensile strength steel and of mild steel to fatigue when notches are present. He used the concepts of notch strain analysis and residual stresses, which were more fully developed later by others [3].

During the 1930s, an important practical advance was achieved by the introduction of shot-peening in the automobile industry. Fatigue failures of springs and axles, which had been common, thereafter became rare. Ahnen; correctly explained the spectacular improvements by compressive residual stresses produced in the surface layers of peened parts, and promoted the use of peening and other processes that produce beneficial residual stresses. Horger showed that surface rolling could prevent the growth of cracks. In 1937 Neuber introduced stress gradient effects at notches and the elementary block concept, which states that the average stress over a small volume at the root of the notch is more important than the peak stress at the notch. In 1939, Gassner emphasized the importance of variable .amplitude testing and promoted the use of an eight-step block loading spectrum for simulated testing. Block testing was prominent until closed-loop electrohydraulic test systems became available in the late 1950s and early 1960s [3].

In 1945, Miner formulated a linear cumulative fatigue damage criterion suggested by Pahngren in 1924. This criterion is now recognized as the Palmgren-Miner linear damage rule. It has been used extensively in fatigue design and, despite its many shortcomings, remains an important tool in fatigue life predictions. The formation of the American Society for Testing and Materials (ASTM) Committee E-09 on Fatigue in 1946, with Peterson' as its first chairman, provided a forum for fatigue testing standards and research. Peterson emphasized that the fatigue notch factor, K_f, was a function of the theoretical stress concentration factor, K_t, the notch and component geometry, and the ultimate tensile strength. In 1953 he published a comprehensive book on stress concentration factors and an expanded version in 1974.

In the period 1945-1960 the foundations of the Low-Cycle-Fatigue were established due to the contributions of Coffin and Manson (1955). Motivated by the aircraft industry, the “fail safe” and “safe life” design approaches were discussed. Miner’s rule was intensively investigated to verify its validity and alternative rules were proposed to overcome the limitations of the linear damage rule. Irwin in 1958, following the previous works by Griffith, realized that the stress intensity factor was the leading parameter to control the static strength of cracked bodies. This contribution led to the Linear Elastic Fracture Mechanics [3].

After 1960 we assist to the development of the Fracture Mechanics and its application to fatigue. One inevitable contribution is the one proposed by Paris (1962) who first recognized the relation between fatigue and Fracture Mechanics. The so-called Paris relation was a pioneer contribution in this field. After this relation, an uncountable number of crack

propagation relations have been proposed to overcome known limitations of the Paris relation. Elber (1963) gave also an important contribution for the understanding of fatigue crack growth under variable amplitude loading, introducing the “crack closure” concept. With the development of fracture mechanics, “damage tolerance” design was adopted in some structures, particularly in Aeronautics [3].

During the 1980s and 1990s, many researchers were investigating the complex problem of in-phase and out-of-phase multiaxial fatigue. The critical plane method suggested by Brown and Miller" motivated a new philosophy concerning this problem, and many additional critical plane models were developed. The small crack problem was noted during this time, and many workers attempted to understand the behaviour. The small crack problem was complex and important, since these cracks grew faster than longer cracks based upon the same driving force. Definitions became very confusing. Interest in the fatigue of electronic materials increased, along with significant research on thermomechanical fatigue. Also during the 1980s and 1990s, significant changes in many aspects of fatigue design were attributed to advances in computer technology. These included software for different fatigue life (durability) models and advances in the ability to simulate real loadings under variable amplitude conditions with specimens, components, or full-scale structures. This brought significantly more field testing into the laboratory. Integrated CAE involving dynamic simulation, finite element analysis, and life prediction/estimation models created the idea of restricting testing to component durability rather than using it for development. Increased digital prototyping with less testing has become a goal of twenty-first-century fatigue design. Despite the very significant advances in fatigue understanding and the current fatigue design practice for structures and mechanical components under dynamic loads, many topics require more research [4].

2.2 Nature of Fatigue

Metals when subjected to repeated cyclic load exhibit damage by fatigue. The magnitude of stress in each cycle is not sufficient to cause failure with a single cycle. Large number of cycles are therefore needed for failure by fatigue. Fatigue manifests in the form of initiation or nucleation of a crack followed by its growth until the critical crack size of the parent metal under the operating load is reached leading to rupture. Behaviour of metal under cyclic load differs from that under monotonic load. New cracks can nucleate during cyclic load that does not happen under static monotonic load. Importantly, fatigue crack nucleates and grows at stress levels far below the monotonic tensile strength of the metal. The crack advances continuously by very small amounts, its growth rate decided by the magnitude of load and geometry of the component. Also the nucleated crack may not grow at all or may propagate extremely slowly resulting in high fatigue life of the component if the applied stress is less than the metal fatigue limit. However, maintaining that condition in actual working components with design constraints and discontinuities calls for limited service loads which may be an impediment. Therefore, fatigue cracks in most cases are permissible but with proper knowledge of fracture mechanics about the allowable or critical crack size. The component under cyclic load can work satisfactorily for years, albeit with hidden crack

growth, but ruptures suddenly without any pre-warning. Such characteristics make cyclic load more dangerous than monotonic load [5].

As stated before, fatigue life until failure consists of two periods: the crack initiation period and the crack growth period as shown in Figure 8. Differentiating between the two periods is of great importance because several surface conditions do affect the initiation period, but have a negligible influence on the crack growth period. The stress concentration factor, K_t, is the important parameter for predictions on crack initiation. The stress intensity factor, K, is used for predictions on crack growth.

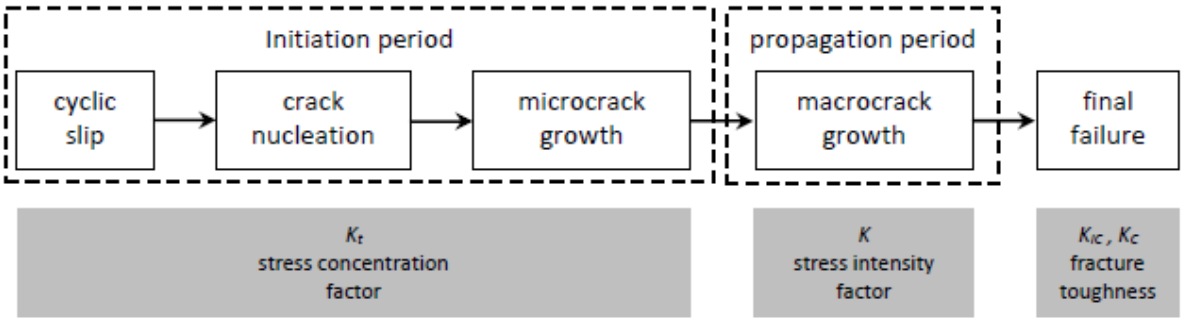

Figure 8. Fatigue life stages [6].

2.3 Factors Influencing Fatigue Life

The factors that influence the fatigue life prediction of materials and structures are the following:

a) Metal microstructure: Metal with large grains have low yield strength and reduced fatigue limit and vice-versa. However, at higher temperatures, the coarse grained metal is seen to show better fatigue properties. Barriers to crack growth in the form of precipitates, impurities, grain boundaries, etc. improve fatigue properties. Phase transformations occurring during cyclic loading can also influence the fatigue life.

b) Manufacturing process: Fatigue properties are better in the direction of forging, extrusion and rolling and are lower in the transverse direction. Some specific processes like shot peening, cold rolling etc. and other hardening/heat treatment methods that induce compressive residual stresses reduce the chances of crack initiation and enhance the fatigue properties. Tensile residual stresses on the other hand promote crack initiation. Other manufacturing processes like forming, drawing, forging, extrusion, rolling, machining, punching etc., that produce rough surfaces, decrease fatigue life. A rough surface possesses more crack initiation sites due to unevenness and asperities. Polished and ground surfaces on the other hand have excellent high fatigue life due to minimum asperities.

c) Component geometry: Discontinuities such as holes, notches and joints, that are the source of stress risers, facilitate crack initiation. Fatigue life of a notched component is less than that of an un-notched one when subjected to similar loads.

d) Type of environment: Aqueous and corrosive environments promote crack initiation and increase crack growth rate although crack tip blunting and closure due to accumulation of environmental products at crack tip may dip crack growth rate to some extent. But the overall effect of such environments is to enhance crack growth rate. Under high temperature too, fatigue resistance in most metals generally diminishes with increase in crack growth rate due to the effect of creep.

e) Loading condition: Multiaxial loads reduces fatigue life in comparison with uniaxial loads except in the case of pure torsional loading. Mean stress also influences fatigue life. Positive tensile mean stress reduces fatigue life whereas negative mean stress may increase it. The influence of mean stress is more significant in low strain or high cycle fatigue regime [5].

2.4 Fatigue Crack Initiation

Fatigue crack initiation and crack growth are a consequence of cyclic slip in slip bands (Figure 9). It implies cyclic plastic deformation as a result of moving dislocations. Fatigue occurs at stress amplitudes below the yield stress. At such a low stress level, plastic deformation is limited to a small number of grains of the material. This micro-plasticity can occur more easily in grains at the material surface because the surrounding material is present at one side only.

Cyclic slip requires a cyclic shear stress. On a micro scale the shear stress is not homogeneously distributed through the material. The shear stress on crystallographic slip planes differs from grain to grain, depending on the size and shape of the grains, crystallographic orientation of the grains, and elastic anisotropy of the material. In some grains at the material surface, these conditions are more favourable for cyclic slip than in other surface grains. Another significant aspect is that slip during the increase of the load also implies some strain hardening in the slip band. As a consequence, upon unloading a larger shear stress will be present on the same slip band, but now in the reversed direction. Reversed slip will thus preferably occur in the same slip band. As a consequence, reversed slip, although occurring in the same slip band, will occur on adjacent parallel slip planes [5].

The lower restraint on cyclic slip at the material surface has been mentioned as a favourable condition for crack initiation at the free surface. However, more arguments for crack initiation at the material surface are present. A very practical reason is the inhomogeneous stress distribution due to a notch effect of a hole or some other geometric discontinuity. Because of an inhomogeneous stress distribution, a peak stress occurs at the surface (stress concentration). Furthermore, surface roughness also promotes crack initiation at the material

surface. Within the light of the discussions it can be concluded that the crack initiation period fatigue is a material surface phenomenon.

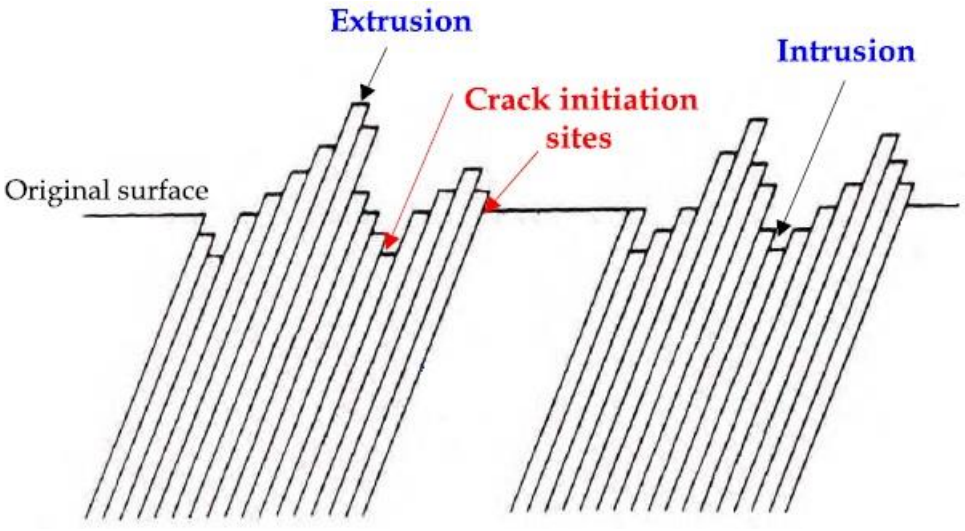

Figure 9. Crack occurrence in cyclic loading [5].

2.5 Fatigue Growth

As long as the size of the microcrack is still in the order of a single grain, the microcrack is obviously present in an elastically anisotropic material with a crystalline structure and a number of different slip systems. The microcrack contributes to an inhomogeneous stress distribution on a micro level, with a stress concentration at the tip of the microcrack. As a result, more than one slip system may be activated. Moreover, if the crack is growing into the material in some adjacent grains, the constraint on slip displacements will increase due to the presence of the neighbouring grains. Similarly, it will become increasingly difficult to accommodate the slip displacements by a single slip system only such as parallel crystallographic planes. It should occur on slip planes in different directions. The microcrack growth direction will then deviate from the initial slip band orientation [6]. In general, there is a tendency to grow perpendicular to the loading direction (Figure 10).

The microcrack growth is dependent on cyclic plasticity; barriers to slip can imply a threshold for crack growth. In the literature, several observations are reported on initially inhomogeneous microcrack growth, which starts with a relatively high crack growth rate and then slows down or even stops due to material structural barriers. Two important surface aspects are no longer relevant. The lower restraint on cyclic slip at the surface is not applicable at the interior of the material, where inclusions or other kind of irregularities may act as trigger for crack initiation. Secondly, surface roughness and other surface conditions do not affect crack growth. Crack growth resistance, when the crack penetrates into the material, depends on the material as a bulk property [4].

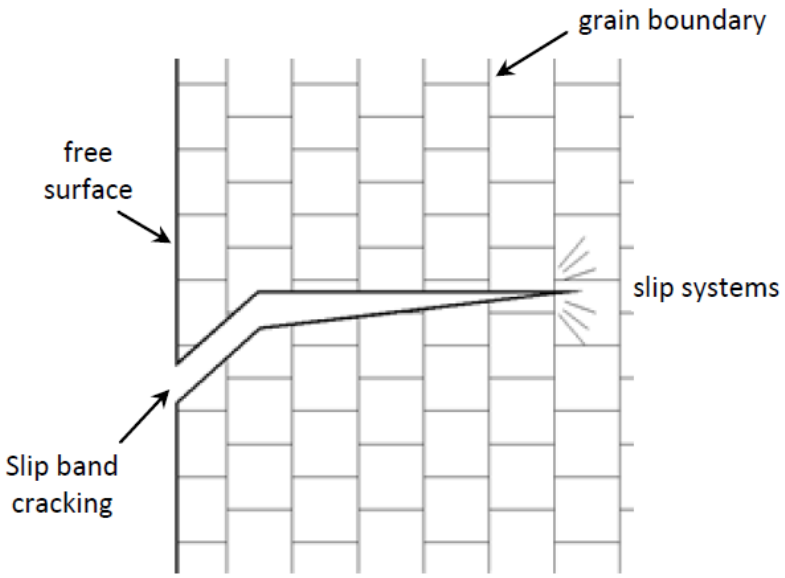

Figure 10. Fatigue crack growth [6].

2.6 Fatigue Life Prediction Methods

In this section an overview is given of different fatigue life prediction models. Since it falls beyond the scope of this study to provide a general overview of all existing fatigue modelling techniques, this overview is limited to stress-life and local strain fatigue models. These techniques can be grouped into the following categories:

- Stress-life approach;
- Local strain models;
- Fracture mechanics;
- Multiaxial models.

The stress-life approach was the first fatigue prediction technique to be developed. This technique is generally used to predict the total life of a component. Local strain models, however, only consider the crack initiation life. This approach can be used when crack initiation dominates the total fatigue life. On the other hand, fracture mechanics only deals with the crack propagation stage. When both the crack initiation and propagation stage of a component are important, local strain models can be used in conjunction with fracture mechanics to predict the total fatigue life by simply adding the calculated number of cycles in the two stages.

Multiaxial fatigue models take into account the multiaxial stress or strain distribution at notches or crack tips and can either be based on a stress or strain based approach or can be based on energetic criteria. Depending on the criterion, the models predict fatigue crack initiation, propagation or total fatigue life.

2.6.1 Stress-life approach

2.6.1.1 *S-N* curves

The stress-life approach is the oldest among the fatigue analysis techniques. This method was developed by Wohler and is based on experimental observations. The mathematical relations of this approach are derived from the so-called *S-N* curve or Wohler curve of which an example is shown in Figure 10. This curve is obtained by subjecting a number of test specimens to fatigue tests at different stress levels. During a single test, the load is fluctuated with a constant amplitude until failure occurs. How failure is defined, depends on the test specimen. For standardized strip- or bar-like specimens, failure means commonly total fracture of the specimen, while for tubular specimens a through-wall crack is generally considered as failure. The resulting number of load cycles to failure N corresponding with a certain stress amplitude S_a is then plotted in the *S-N* curve. The number of cycles N is plotted on the horizontal axis, which is conventionally put in logarithmic scale. The stress amplitude on the vertical axis can be either logarithmically or linearly plotted.

A typical example of an *S-N* curve is shown in Figure 11. It starts as a sloping curve changing into a horizontal asymptote with the number of cycles to failure becoming infinite. The stress level corresponding to the asymptote is referred to as the *fatigue limit.* Since stresses below the fatigue limit would never result in fatigue failure, tests are generally stopped when a certain number of cycles is reached, for example at 2×10^6 cycles.

Fatigue test data are prone to scatter, due to the nature of the fatigue mechanism. Nevertheless, the data can be embedded in a certain fatigue- fracture band wherein the probability of failure changes from a low probability next to the finite-life region, to a high probability next to the fracture region. Typically a mean curve for the finite-life region with a 50 % probability of failure is used according to the Basquin relation [7]:

$$S_a^k \cdot N = \text{constant} \tag{2.1}$$

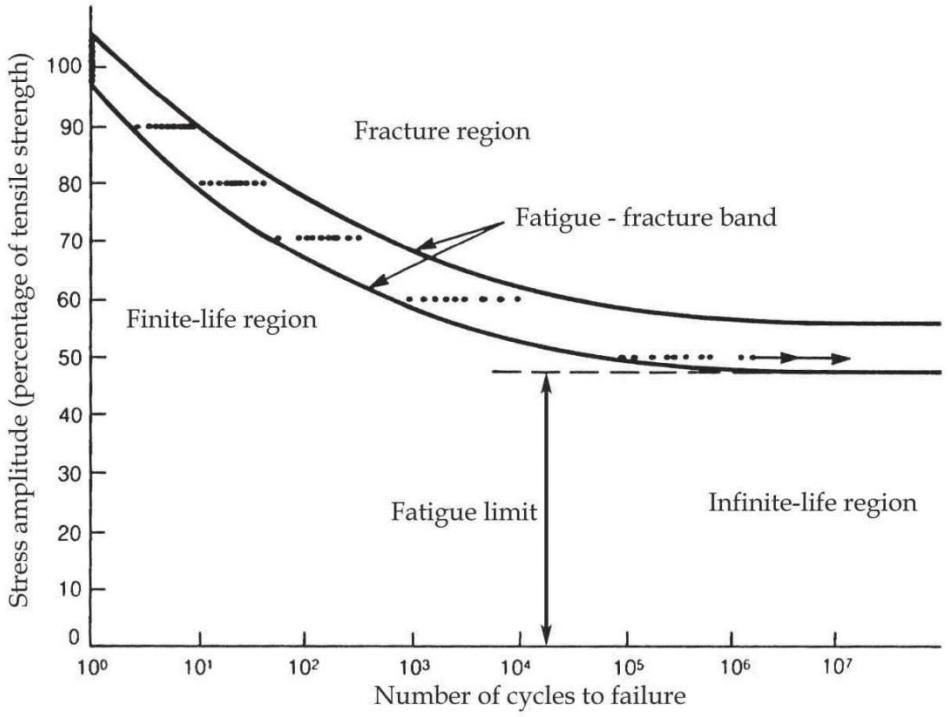

Figure 11. Typical S-N curve of a medium-strength steel.

For design purposes a probability of failure of 50 % is obviously unacceptable. For this reason design curves are used which are obtained by subtracting two times the standard deviation from the mean curve which corresponds to a probability of failure of 4.55 %.

The stress amplitude to which the fatigue life is related to is generally a nominal stress, since it is derived from the forces applied in the experimental test setup. This has the advantage of avoiding complex stress analysis evaluate the test specimens. However, this means that results obtained for a specific component cannot easily be extended to a modified component. Additionally, *S-N* curves are obtained from constant amplitude tests whereas in practice most components are subjected to variable amplitude stresses. To use *S-N* data for practical load histories, the cumulative fatigue damage model of Miner [8] can be used:

$$D = \sum_i \frac{n_i}{N_i} \tag{2.2}$$

Miner postulated that fatigue damage accumulates linearly. When a component is subjected to n_i stress cycles at a stress which has N_i cycles to failure, then a fraction of n_i/N_i of the total life is consumed. The damage accumulated over the cycles at different stress levels is summed up to give the total damage D. The component would fail if D becomes one. Miner's theory assumes that damage can be superimposed, that the appearing damage is irreversible and that there is no interaction between different stress

levels in the sense that it is unimportant in which order the component experiences the stress cycles.

2.6.1.2 Mean stress effect

Fatigue tests can be carried out with a fully reversible load with zero mean stress or with a fluctuating load with a certain prestress. To make the test conditions clear, a load ratio R as defined by Eq. (2.3) should be mentioned with every S-N curve. Additionally, S_r is the applied stress range and S_m is the mean stress.

$$R = \frac{S_{min}}{S_{max}} \tag{2.3}$$

where S_{min} and S_{max} are respectively the minimum and maximum applied stress, as shown in Figure 12.

Many *S-N* curves are given for a fully reversible fatigue load with zero mean stress or load ratio R = -1. In order to compare data obtained in tests conducted at a different load ratio, the Goodman Eq. (2.4) can be used to correct the mean stress effect.

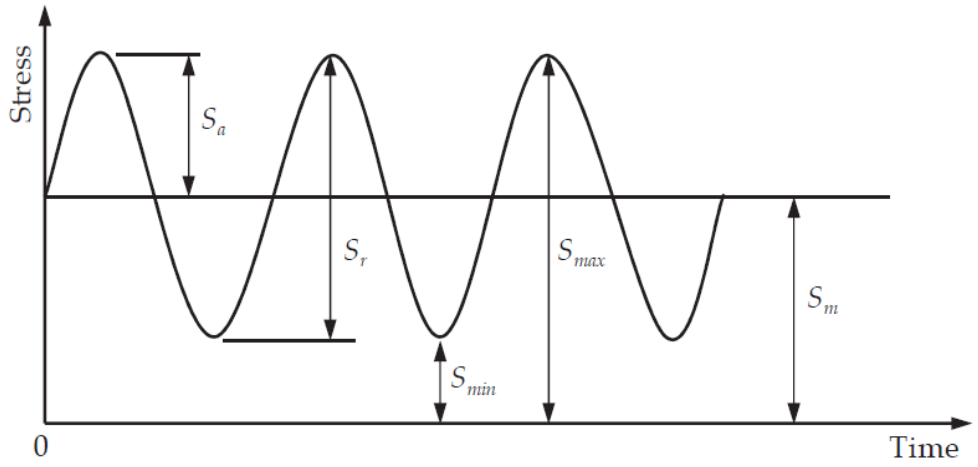

Figure 12. Stress definitions.

With this equation the fatigue stress S_f as would occur for a fully reversible fatigue load can be calculated from the applied stress amplitude S_a taking into account the ratio between the applied mean stress S_m and the material's tensile strength σ_{UTS}.

$$\frac{S_a}{S_f} = 1 - \frac{S_m}{\sigma_{UTS}} \tag{2.4}$$

2.6.1.3 Stress concentrations

To determine the fatigue life of a machined component, the fatigue data of standard test specimens can be used. However, a real-life component has an arbitrary size with a certain stress concentration, an arbitrary surface finish and an arbitrary loading mode, while standard test specimens have prescribed dimensions and a polished surface. To take all these differences into account, the fatigue stress of the machined component $S_{f,comp}$ can be estimated from the fatigue stress of a standard component S_f by introducing a number of correction factors:

$$S_{f,comp} = k_a k_b k_c \frac{S_f}{K_f} \tag{2.5}$$

In this equation k_a is a correction factor for the loading mode, since the fatigue behaviour of a component is different when the loads are applied e.g. in tension or bending mode. The factor k_b deals with the size effect, which takes into account that the effect of fatigue failure on small standardized specimens can be different from the effect on a bigger structure. k_c is a surface roughness factor that allows to relate the results of polished standard specimens to machined parts with a higher surface roughness. Finally, K_f is the fatigue notch factor. This can be calculated from the geometrical stress concentration factor K_t by Eq. (2.6) with q the notch sensitivity factor.

$$K_f = 1 + q(K_t - 1) \tag{2.6}$$

When using this technique to evaluate threaded connections based on experimental data of the pipeline steel, one should consider that the factors k_a, k_b, k_c and q are all given by empirical relations or charts, which means that each single factor is subjected to a certain amount of uncertainty. Additionally, the input for these relations or charts requires measurements of local parameters such as surface roughness and root radii. Next to this, selecting a certain uniaxial loading mode from a complex stress distribution might be an oversimplification. Due to these assumptions and the scatter of every factor, the calculated life might differ significantly from the real behaviour of the connection.

2.6.2 Local Approaches

Fatigue design philosophy has evolved from fatigue limit and infinite life criteria to approaches based on finite life behaviour. The local approaches use fatigue damage parameters to correlate fatigue test results, especially for crack initiation life. In order to predict the fatigue life under a specified condition, different fatigue damage parameters have been proposed to correlate fatigue life. The local approaches are generally divided into three categories, i.e., stress-based, strain-based and energy-based methods, when stress, strain or energy are independently used as the fatigue damage parameter [4]. Models to account for the stress level effect referring to the stress-based, strain-based and energy-based methods have been proposed by different authors. These models are presented in the following.

2.6.2.1 Stress-based method

The stress-life method uses the alternating stress amplitude to predict the number of cycles to failure [4]. This method is based on comparing the stress amplitude to stress amplitude versus fatigue life curve (*S-N* diagram). The *S-N* curves are based on empirical formulas derived from experimental data. The stress-life method is generally only used for high cycle fatigue, because under low cycle fatigue the stress-strain relationship becomes nonlinear. Similar to *S-N* curves, the relation between stress amplitude, $\Delta\sigma/2$, and the number of cycles to failure, N_f, can be approximated by a straight line when the stress amplitude and the fatigue life are both expressed on a logarithmic scale, thus resulting in [7]:

$$\frac{\Delta\sigma}{2} = \sigma'_f \cdot (N_f)^b \tag{2.7}$$

where σ'_f is the fatigue strength coefficient, and b is the fatigue strength exponent. For many loading cases, the mean stress is not zero. Although the stress level effect is often neglected in fatigue life calculations for welded details, the high residual stresses in such details tend to obliterate any possible effect of applied stress level. However, in non-welded details, the effect of stress level must be accounted for in the fatigue life calculations.

Morrow [9] proposed a correction to account for the mean stress effect as follows:

$$\frac{\Delta\sigma}{2} = (\sigma'_f - \sigma_m) \cdot (N_f)^b \tag{2.8}$$

where σ_m is the mean stress and the other variables are the same as for Equation (2.8). The effect of the tensile mean stress is thus equivalent to a reduction of the fatigue strength coefficient. The model assumes that a given combination of stress amplitude, $\Delta\sigma/2$, and mean stress, σ_m, is expected to have the same fatigue life as a fully reversed stress amplitude of $\left(\frac{\Delta\sigma}{2}\right)_{-1}$, where:

$$\left(\frac{\Delta\sigma}{2}\right)_{-1} = \frac{\frac{\Delta\sigma}{2}}{1 - \frac{\sigma_m}{\sigma'_f}} \tag{2.9}$$

The Morrow correction for stress-based method was found to work reasonably well for structural grades of steels.

2.6.2.2 Strain Based Approach

The strain-based approach to fatigue problems is widely used at present. Strain can be measured and has been shown to be an excellent quantity for correlating with low-cycle

fatigue. For example, gas turbines operate at fairly steady stresses, but when they are started or stopped, they are subjected to a very high stress range. The local strains can be well above the yield strain, and the stresses are more difficult to measure or estimate than the strains. The most common application of the strain-based approach, however, is in fatigue of notched members. In a notched component or specimen subjected to cyclic external loads, the behaviour of material at the root of the notch is best considered in terms of strain. As long as there is elastic constraint surrounding a local plastic zone at the notch, the strains can be calculated more easily than the stress [3]. This concept has motivated the strain-life design method based on relating the fatigue life of notched parts to the life of small, unnotched specimens that are cycled to the same strains as the material at the notch root. Since fatigue damage is assessed directly in terms of local strain, this approach is called the "local strain approach". A reasonable expected fatigue life, based on the nucleation or formation of small macrocracks, can then be determined if one knows the local strain-time history at a notch in a component and the unnotched strain-life fatigue properties of the material. The remaining fatigue crack growth life of a component can be analysed using fracture mechanics concepts.

For engineering materials at room temperature, cyclic hardening or softening usually takes place rapidly at first and then approaches to a stable condition. The stable cyclic stress versus strain curve is often defined using the Ramberg-Osgood equation [10]. The curve can be determined from several companion specimens cycled at various constant strain amplitudes or from a single specimen in conformity with the incremental step test method.

The total strain amplitude in Figure 13 can be resolved into elastic and plastic strain components from the steady-state hysteresis loops. At a given life, N_1, the total strain is the sum of the elastic and plastic strains. Both the elastic and plastic curves can be approximated as straight lines. At large strains or short lives the plastic strain component is predominant, and at small strains or longer lives the elastic strain component is predominant.

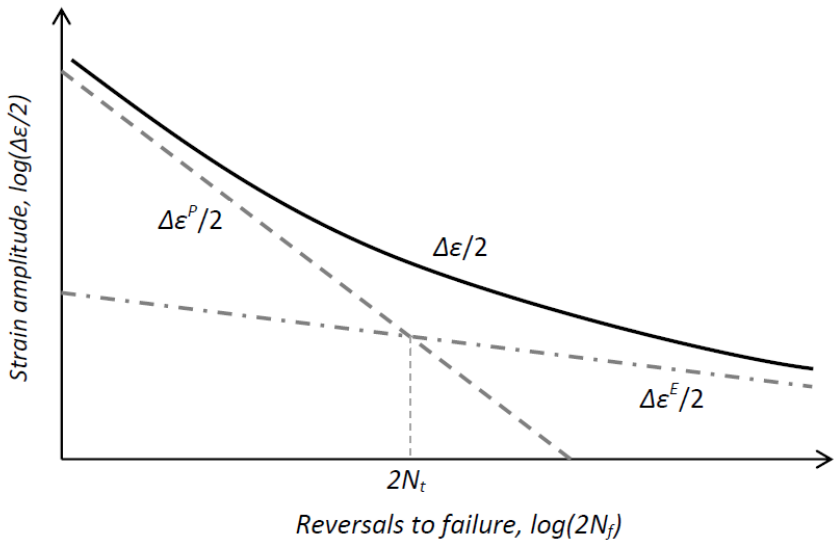

Figure 13. Strain-life curves showing total, elastic, and plastic strain components.

Basquin's equation [7], proposed in 1910, which represent the elastic component of the strain amplitude, ${\Delta\varepsilon^E}/{2}$, can be obtained as follows:

$$\frac{\Delta\varepsilon^E}{2} = \frac{\sigma'_f}{E}(N_f)^b \tag{2.10}$$

The plastic strain amplitude, ${\Delta\varepsilon^P}/{2}$, versus fatigue life can also be linearized on a logarithmic scale for low cycle fatigue. The relationship between the plastic strain amplitude and fatigue crack initiation life can be expressed in the following form which is known as Manson-Coffin relationship [11,12] proposed in the early 1960s:

$$\frac{\Delta\varepsilon^P}{2} = \varepsilon'_f(N_f)^c \tag{2.11}$$

where ε'_f is the fatigue ductility coefficient, and c is the fatigue ductility exponent, both determined experimentally. By adding the elastic and plastic components of strain amplitude, given respectively by Equations (2.10) and (2.11), the relationship between the total strain amplitude, ${\Delta\varepsilon}/{2}$, and fatigue life can be expressed as:

$$\frac{\Delta\varepsilon}{2} = \frac{\Delta\varepsilon^E}{2} + \frac{\Delta\varepsilon^P}{2} = \frac{\sigma'_f}{E}(N_f)^b + \varepsilon'_f(N_f)^c \tag{2.12}$$

The life at which elastic and plastic components of strain are equal is called the "transition fatigue life", $2N_t$. This is the life at which the elastic and plastic strain-life curves intersect.

In strain-controlled cycling with a mean strain usually results in a mean stress, which may relax fully or partially with continued cycling, as shown in Figure 14. This relaxation is due to the presence of plastic deformation, and therefore, the rate or amount of relaxation depends on the magnitude of the plastic strain amplitude. As a result, there is more mean stress relaxation at larger strain amplitudes. Mean strain does not usually affect fatigue behaviour unless it results in a non-fully relaxed mean stress. Since there is more mean stress relaxation at higher strain amplitudes due to larger plastic strains, mean stress effect on fatigue life is smaller in the low-cycle fatigue region and larger in the high cycle fatigue region. The inclusion of mean stress effects in fatigue life prediction methods involving strain-life data is more complex. Several models dealing with mean stress effects on strain-life fatigue behaviour are discussed in. One method, often referred to as "Morrow's mean stress method", replaces σ'_f with $(\sigma'_f - \sigma_m)$ in Eq. 2.12, where σ_m is the mean stress, such that [9]:

$$\frac{\Delta\varepsilon}{2} = \varepsilon_a = \frac{(\sigma'_f - \sigma_m)}{E} \cdot (2N_f)^b + \varepsilon'_f(2N_f)^c \tag{2.13}$$

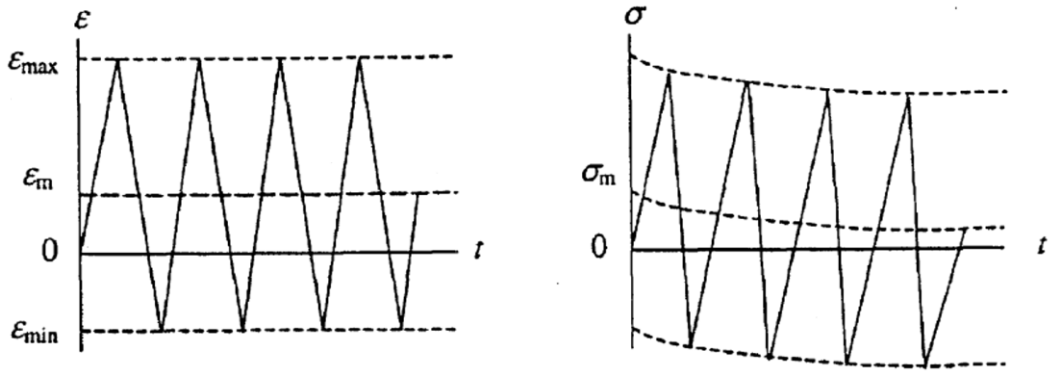

Figure 14. Mean stress relaxation under strain-controlled cycling with a mean strain [3].

An alternative version of Morrow's mean stress parameter where both the elastic and plastic terms are affected by the mean stress is given by Manson:

$$\frac{\Delta\varepsilon}{2} = \varepsilon_a = \frac{(\sigma'_f - \sigma_m)}{E} \cdot (2N_f)^b + \varepsilon'_f \left(\frac{\sigma'_f - \sigma_m}{\sigma'_f}\right)^{\frac{c}{b}} (2N_f)^c \tag{2.14}$$

Another equation suggested by Smith, Watson, and Topper [13] (often called the "*SWT* parameter"), based on strain-life test data obtained with various mean stresses, is

$$\sigma_{max}\,\varepsilon_a = \frac{(\sigma'_f)^2}{E} \cdot (2N_f)^{2b} + \sigma'_f \varepsilon'_f (2N_f)^{b+c} \tag{2.15}$$

where $\sigma_{max} = \sigma_m + \sigma_a$ and ε_a is the alternating strain. This equation is based on the assumption that for different combinations of strain amplitude, ε_a, and mean stress, σ_{max} the product $\sigma_{max}\,\varepsilon_a$ remains constant for a given life.

2.6.3 Multiaxial Fatigue Approaches

When dealing with structures subjected to complex load cases, the above mentioned fatigue analysis approaches, might not give accurate results since they consider the dynamic loads to be uniaxial. Even in situations where the global acting stress is purely uniaxial, the local stress situation around notches or irregularities can be multiaxial. To describe such load cases more accurately, multiaxial fatigue models were developed.

The origin of multiaxiality in stress is dependent on various parameters such as type of loading, complex geometry of the mechanical parts, residual stresses or pre-stresses, etc. In order to estimate fatigue strength of the components, many multiaxial fatigue criteria have been proposed in the literature for metals. From technical point of view, multiaxial criteria for prediction of fatigue strength of mechanical components may be categorized into three

main groups, namely stress based criteria, strain based criteria and energy based approaches. As for the stress criteria proposed by Susmel and Lazzarin, McDiarmid, Crossland and so on, are based only on stress and are suitable for high cycle fatigue when the deformation is elastic or the plastic strain is small. The strain criteria such as the Brown–Miller model, Fatemi–Socie, Li–Zhang and Wang–Brown model, are appropriate for such cases in which there is significant plasticity. The energy based multiaxial criteria such as the Smith–Watson–Topper model, Glinka and Varani-Farahani include both stress and strain terms.

Multiaxial fatigue criteria, from another point of view, can be categorized as those criteria which use the critical plane concept and those do not use this concept. In the multiaxial fatigue criteria based on critical plane, initially a material plane on which a combination of some stress components has the maximum value has been determined. Then, fatigue parameters as combinations of the maximum shear strain or stress and normal strain or stress on the critical plane have been calculated. The criteria will be checked then on this plane. Like to classical models, critical plane models can be stress-, strain- or energy-based. The concept of critical planes was primarily proposed by Brown and Miller. Brown and Miller proposed a strain-based parameter that considers that fatigue life to be a non-linear function of strain. The critical plane of this parameter is the plane of maximum shear strain. Firstly, the history of strain on the critical plane is analysed; and then strain parameters are used to quantify the damage parameters on the critical plane. Various terms have been proposed for different materials and experimental results. Socie proposed that the fatigue life criterion should be based on a physical mechanism. Socie modified the SWT parameter for a material with tensile-type failures, by taking the view that crack growth is perpendicular to the maximum tensile stress.

The energy criteria have been used in conjunction with the critical plane approach, as proposed by Liu, and Glinka. Varani-Farahani (VF) proposed critical plane based energy parameters that are weighted by axial and shear fatigue properties of the material. In fact, many efforts have been made to evaluate the performance of multiaxial fatigue criteria for various materials, notched and unnotched components, different loading conditions and stress (and strain) states by several authors such as Papadopoulos *et al.*, Sonsino, Brown and Miller, You and Lee, Macha and Sonsino, Wang and Yao, Chakherlou and Abazadeh, Varvani-Farahani *et al.*, and Jiang *et al*. However, due to the complexity of this challenging problem and its practical application, much additional studies are still needed to evaluate the accuracy and reliability of the multiaxial fatigue criteria in design, life estimation, and failure assessment particularly for practical specimens [14]. Some multiaxial fatigue life estimation methods for bolted connections were presented below.

2.6.3.1 Stress-based fatigue criteria

Gough and Pollard [15,16] proposed for ductile metals under combined in-phase bending and torsion the following equation for the fatigue limit under combined multiaxial stresses:

$$\left(\frac{\sigma_b}{\sigma_{FL}}\right)^2 + \left(\frac{\tau_t}{\tau_{FL}}\right)^2 = 1 \qquad (2.16)$$

Sines [17] proposed an alternative criterion in high-cycle fatigue regime, which became very popular:

$$\sqrt{J_{2,a}} + k\sigma_{H,m} \leq \lambda \tag{2.17}$$

A similar criterion was proposed by Findley [18], Matake [19] and McDiarmid [20] using the shear stress amplitude and the maximum normal stress on the critical plane as parameters:

$$\tau_{a,cr} + k\sigma_{n,cr} \leq \lambda \tag{2.18}$$

McDiarmid [20] defined k and λ as follows:

$$k = \frac{t_{A,B}}{2\sigma_u}, \lambda = t_{A,B} \tag{2.19}$$

Papadopoulos [21] proposed a fatigue limit criterion which could be used in constant amplitude multiaxial proportional and non-proportional loading in high-cycle fatigue regime:

$$\tau_{a,cr} + k\sigma_{H,max} = \lambda \tag{2.20}$$

Crossland's criterion [22] uses the square root from the second invariant of stress tensor. This invariant is determined from the stress amplitude. Another term added to the equation is the hydrostatic stress calculated from maximal stress values.

$$a_c \cdot \sqrt{J_{2,a}} + b_c \cdot \sigma_{H,max} \leq f_{-1} \tag{2.21}$$

The Crossland criterion [22] is a stress based multiaxial fatigue criterion which uses the second invariant of deviatoric stress tensor and maximum hydrostatic stress in its equation.

$$\sqrt{J_{2,a}} + k \cdot \sigma_{H,max} = \sigma_f'\left(2N_f\right)^b \tag{2.22}$$

$$\sqrt{J_{2,a}} = \frac{1}{2\sqrt{6}}[(\Delta\sigma_1 - \Delta\sigma_2)^2 + (\Delta\sigma_2 - \Delta\sigma_3)^2 + (\Delta\sigma_1 - \Delta\sigma_3)^2]^{1/2} \tag{2.23}$$

where $J_{2,a}$ is the amplitude of second invariant of deviatoric stress tensor and $\sigma_{H,max}$ is the maximum value of the hydrostatic stress (sum of the mean and amplitude values of the hydrostatic stress). Also k is a material dependent constant.

2.6.3.2 Strain-based type criteria

Findley and Tracy [23, 24] proposed a fatigue life equation in low-cycle fatigue regime about the influence of normal stresses to the maximum shear stress plane, with the following form:

$$\left(k \cdot \sigma_n + \frac{\Delta\tau}{2}\right)_{max} = \tau_f^* (N_f)^b \tag{2.24}$$

where k is a material constant, $\Delta\tau/2$ ($=\tau_a$) is the alternating shear stress, $\sigma_{n,max}$ is the maximum normal stress, and variable τ_f^* is determined using the torsional fatigue strength coefficient, τ_f^*, in the equation:

$$\tau_f^* = \sqrt{1+k^2} \cdot \tau_f' \tag{2.25}$$

Brown and Miller [25] defined the damage critical plane and proposed the following equation:

$$\left(S \cdot \Delta\varepsilon_n + \frac{\Delta\tau}{2}\right)_{max} = A\frac{\sigma_f'}{E}(2N_f)^b + B\varepsilon_f'(2N_f)^c \tag{2.26}$$

with

$$A = 1.3 + 0.7S \; and \; B = 1.5 + 0.5S \tag{2.27}$$

where S is a Brown and Miller constant.

Fatemi and Socie [26] proposed a strain-based parameter that considers the plane of maximum shear strain amplitude as a critical plane. Fatemi–Socie fatigue model is expressed as

$$\frac{\Delta\gamma_{max}}{2}\left(1 + k\frac{\sigma_{n,max}}{\sigma_y}\right) = \frac{\tau_f'}{2G}(2N_f)^{b'} + \gamma_f'(2N_f)^{c'} \tag{2.28}$$

where $\Delta\gamma_{max}$ is the maximum shear strain and $\sigma_{n,max}$ is the maximum normal on the plane that $\Delta\gamma_{max}$ occurs. Also k=0.3 is the Fatemi–Socie constant and σ_y is the tensile yield strength which can be obtained from uniaxial and torsional tests. The coefficients τ_f', γ_f' and G are the torsional fatigue strength and ductility coefficients, and the shear modulus respectively. The exponents b' and $c'$are the torsional fatigue strength and ductility exponents, respectively. The physical basis of Fatemi–Socie parameter is shown in Figure 8b. The maximum normal stress term in Fatemi–Socie parameters enable it to include mean stresses.

Kandil, Brown and Miller (KBM) [22] proposed a multiaxial theory based on a physical interpretation of mechanisms of fatigue crack growth. The general form of KBM's parameter is expressed as:

$$\frac{\Delta\gamma_{max}}{2} + S_k\Delta\varepsilon_n = \frac{\sigma_f'}{E}(2N_f)^b + \varepsilon_f'(2N_f)^c \tag{2.29}$$

The critical plane of this parameter is the plane of maximum shear strain, where $\Delta\gamma_{max}$ the maximum is shear strain range and $\Delta\varepsilon_n$ is the corresponding normal strain range at the critical plane. Also, S_k is a material dependent constant which is chosen so that the equation gives the same fatigue life as for uniaxial stresses. These values can be determined with principal stresses and strains obtained from finite element analyses, and therefore, using Eqs. (2.30) and (2.31) for nodes around the bolt hole. In Eqs. (2.30) and (2.31), ε_1, and ε_3, are the first and third principal strains respectively. In addition, θ_1 and θ_2 in these equations are indicating loading and unloading of a cycle. These parameters are determined for every node around the hole and the maximum value of the left hand side of Eq. (2.32) is used to predict the fatigue life of the specimens.

$$\frac{\Delta\gamma}{2} = \left(\frac{\varepsilon_1 - \varepsilon_3}{2}\right)_{\theta_1} - \left(\frac{\varepsilon_1 - \varepsilon_3}{2}\right)_{\theta_2} \tag{2.30}$$

$$\frac{\Delta\varepsilon_n}{2} = \left(\frac{\varepsilon_1 + \varepsilon_3}{2}\right)_{\theta_1} - \left(\frac{\varepsilon_1 + \varepsilon_3}{2}\right)_{\theta_2} \tag{2.31}$$

2.6.3.3 Energy-based criteria

Smith et *al.* [13] proposed an experimental damage parameter which is evaluated at the plane of maximum normal strain. The *SWT* multiaxial fatigue model is expressed as;

$$\sigma_n^{max}\frac{\Delta\varepsilon_1}{2} = \frac{(\sigma_f')^2}{E}(2N_f)^{2b} + \sigma_f'\varepsilon_f'(2N_f)^{b+c} \tag{2.32}$$

where σ_n^{max} and ε_1 are the maximum normal stress and the maximum principal strain range at the critical plane. A schematic that illustrates the physical basis of *SWT* parameter is shown in Figure 15a. In this study the maximum value of the product, ($\sigma_n^{max}\frac{\Delta\varepsilon_1}{2}$) in any node has been used. To do so, σ_n^{max} (maximum normal stress) and ε_1 (first principal strain range) have been calculated during cyclic loading in any node of the FE models and consequently the maximum amount of the product of these two parameters has been employed in Eq. (2.32) to calculate the estimated fatigue life.

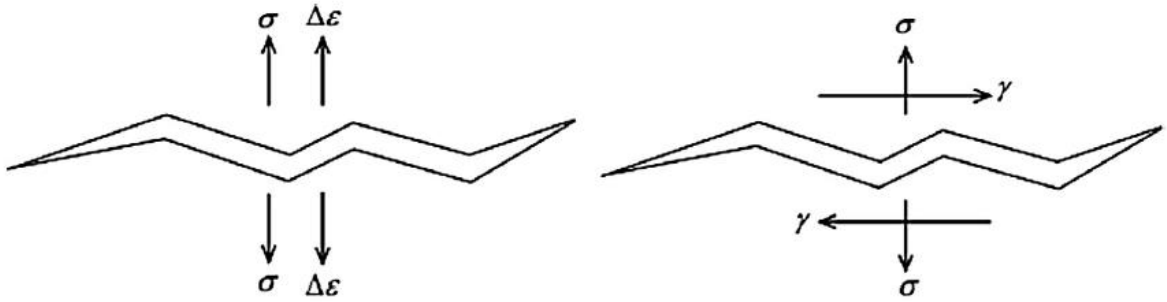

(a) (b)

Figure 15. Crack growth: (a) tensile crack growth according to *SWT* criterion and (b) effect of normal stress on shear crack growth according to FS criterion.

where σ_n is the maximum principal stress during the cycle and $\Delta\varepsilon_1/2$ is the principal strain amplitude. Socie [27] modified the *SWT* parameter taking into account the parameters that control the damage, such as:

$$SWT = \Delta\varepsilon_1^{max} \cdot \Delta\sigma_1 + \Delta\gamma_1^{max} \cdot \Delta\tau_1, for\ tensile\ mode \tag{2.33}$$

$$SWT = \Delta\gamma_{max} \cdot \Delta\tau \quad + \Delta\varepsilon_n \ \cdot \Delta\sigma_n, for\ shear\ mode \tag{2.34}$$

Other approaches for the *SWT* parameter were proposed by Chu et *al.* [28], Liu [29] and Glinka et *al.* [30]. Ellyin [31] proposed a model based on the energy density associated to each cycle, ΔW^t, which is composed by two parts: plastic strain energy, ΔW^P, and the positive elastic strain energy, ΔW^{E+}. In the case of proportional or biaxial non-proportional loading, the total energy density associated to a cycle may be computed as:

$$\Delta W^t = \Delta W^P + \Delta W^{E+} = \int_t^{t+T} \sigma_{ij} d\varepsilon_{ij}^P + \int_t^{t+T} H(\sigma_i) H(d\varepsilon_i^e) \sigma_i d\varepsilon_i^e \tag{2.35}$$

where σ_{ij} and ε_{ij}^P are the stress and plastic strain tensors, σ_i and ε_i^e are the principal stresses and the principal elastic strains, T is the period of one cycle and *H(x)* is the Heaviside function. The fatigue failure criterion is defined according to the following expression:

$$\psi = \Delta W^t = \frac{\Delta W^P}{\bar{\rho}} + \Delta W^{E+} = \kappa\left(2N_f\right)^{\alpha} + C \tag{2.36}$$

where κ, α and C are material parameters to be determined from appropriate tests and $2N_f$ is the number of reversals to failure. The multiaxial constraint ratio, $\bar{\rho}$, can be determined using the following expression:

$$\bar{\rho} = (1 + \bar{\nu}) \frac{\hat{\varepsilon}_{max}}{\hat{\gamma}_{max}} \tag{2.37}$$

with

$$\hat{\varepsilon}_{max} = max[\varepsilon_a, \varepsilon_t] \tag{2.38}$$

$$\hat{\gamma}_{max} = max[|\varepsilon_a - \varepsilon_r|, |\varepsilon_t - \varepsilon_r|] \tag{2.39}$$

where ε_a and ε_t are principal in-plane strain (axial and transversal) parallel to the free surface, ε_r is the radial strain (perpendicular to the free surface), and $\bar{\nu}$ is an effective Poisson's ratio.

Glinka et *al.* [22] proposed a fatigue parameter by using the summation of elastic and plastic energy densities on the critical shear plane.

$$\frac{\Delta\gamma}{2} \cdot \frac{\Delta\tau}{2} + \frac{\Delta\varepsilon_n}{2} \cdot \frac{\Delta\sigma_n}{2} = \frac{(\sigma_f')^2}{E} (2N_f)^{2b} + \frac{E\varepsilon_f'}{2} (2N_f)^{b+c} \tag{2.40}$$

where $\Delta\gamma$, $\Delta\tau$, $\Delta\varepsilon_n$ and $\Delta\sigma_n$ are the range of shear strain, shear stress range, normal strain range and normal stress range on the critical plane respectively. These values can be determined with principal stresses and strains obtained from the finite element analysis, and therefore, using Eqs. (2.30), (2.31), (2.41), and (2.42) for nodes around the bolt hole. The maximum value of the left hand side of Eq. (2.31) among the calculated values of the nodes can be used to predict the fatigue life of specimens.

$$\Delta\tau = \left(\frac{\sigma_1 - \sigma_3}{2}\right)_{\theta_1} - \left(\frac{\sigma_1 - \sigma_3}{2}\right)_{\theta_2} \tag{2.41}$$

$$\Delta\sigma_n = \left(\frac{\sigma_1 + \sigma_3}{2}\right)_{\theta_1} - \left(\frac{\sigma_1 + \sigma_3}{2}\right)_{\theta_2} \tag{2.42}$$

where σ_1, and σ_3 are the biggest and smallest principal stress values respectively.

The Jahed-Varvani (JV) energy-based model [32], that considers the sum of plastic and positive elastic strain energy densities as a measure of fatigue damage is used for fatigue life predictions. As for *SWT* and FS, the JV model includes a mean stress effect and can be used for both proportional and non-proportional loading conditions. This criterion defines the critical plane as the plane where maximum amount of shear strain range occurs and uses normal stress and strain perpendicular to the critical plane and introduces it as fatigue damage parameter. However, the critical plane does not always coincide with the plane where the fatigue damage parameter takes its maximum value. Therefore, the maximum

damage plane on which the fatigue damage parameter assumes its maximum value can be defined as the critical plane.

$$\left[\frac{1}{\sigma_f'\varepsilon_f'}(\Delta\sigma_n\cdot\Delta\varepsilon_n)+\frac{\left(1+\frac{\sigma_n^m}{\sigma_f'}\right)}{\tau_f'\gamma_f'}\left(\frac{\Delta\boldsymbol{\gamma}}{\mathbf{2}}\cdot\frac{\Delta\boldsymbol{\tau}}{\mathbf{2}}\right)\right]_{max}=\frac{\sigma_f'}{E}(2N_f)^b+\varepsilon_f'(2N_f)^c+\frac{\tau_f'}{G}(2N_f)^{b'}+\gamma_f' \qquad (2.43)$$

where the normal mean stress σ_n^m acting on the critical plane is given in [32]:

$$\sigma_n^m=\frac{1}{2}\left(\sigma_n^{max}+\sigma_n^{min}\right) \qquad (2.44)$$

In Eq. (2.43) $\Delta\gamma$ and $\Delta\varepsilon_n$ are calculated from Eqs. (2.40) and (2.41), and σ_n is the normal stress. Eq. (2.43) is then solved for data of the critical node in which the left hand side of the equation achieves its maximum value.

2.6.3.4 Nominal stress approach

The calculation of nominal normal ($\Delta\sigma_{nom}$) and shear ($\Delta\tau_{nom}$) stress ranges using the theory of elasticity are typical when applied with design codes. The fatigue assessment using the nominal stress approach for several joints is shown in fatigue classes where the relation between applied stress range, $\Delta\sigma_{nom}$ or $\Delta\tau_{nom}$, and fatigue life, N, is given by the following relations:

$$N\cdot\Delta\sigma_{nom}^m=C \qquad (2.45)$$

$$N\cdot\Delta\tau_{nom}^{m_\tau}=C_\tau \qquad (2.46)$$

where C, C_τ, m and m_τ are material constants. The material constants m and m_τ describe the slope of the fatigue strength curves.

The normal and shear stresses effects must be combined in the multiaxial fatigue assessment. The Eurocode 3 part 1-9 [33] present three different alternatives to take into account their effects:

i) The effects of the shear stress range may be neglected, if the $\Delta\tau_{nom}<0.15\Delta\sigma_{nom}$;

ii) For proportional loading, the maximum principal stress range may be used, in the situation in that the plane of the maximum principal stress doesn't change significantly in the course of a loading event;

iii) For non-proportional loading events, the components of damage for normal and shear stresses should be assessed separately using the interaction equation or the Palmgren-Miner rule:

$$\left(\frac{\Delta\sigma_{eq,nom}}{\Delta\sigma_c}\right)^3 + \left(\frac{\Delta\tau_{eq,nom}}{\Delta\tau_c}\right)^5 \leq 1 \tag{2.47}$$

where $\Delta\sigma_c$ and $\Delta\tau_c$ are the reference values of the fatigue strength at 2 million cycles.

$$D_\sigma + D_\tau \leq 1 \tag{2.48}$$

The computation of the equivalent normal and shear stress ranges are presented, as a function of the normalized stress cycles, N_{ref}:

$$\Delta\sigma_{eq,nom} = \sqrt[m]{\frac{\sum_{i=1}^{k}\left(\Delta\sigma_{nom,i}^{m}\cdot n_i\right)}{N_{ref}}} \tag{2.49}$$

$$\Delta\tau_{eq,nom} = \sqrt[m_\tau]{\frac{\sum_{i=1}^{k}\left(\Delta\tau_{nom,i}^{m_\tau}\cdot n_i\right)}{N_{ref}}} \tag{2.50}$$

2.6.3.5 Fracture Mechanics criteria

The Fracture Mechanics is based on three cracks deformation modes. These deformation modes are the following: opening mode or tension mode or mode I; in-plane shear or mode II; and out-of-plane shear or mode III.

A simple power law relationship between the rate of the crack growth per cycle (da/dN) and the range of stress intensity factor (ΔK_I) to describe the tension mode for mode I in constant or variable amplitude loading conditions was developed by Paris and Erdogan [34]:

$$\frac{da}{dN} = C(\Delta K_I)^m \tag{2.51}$$

where C and m are material constants (see Fig. 16).

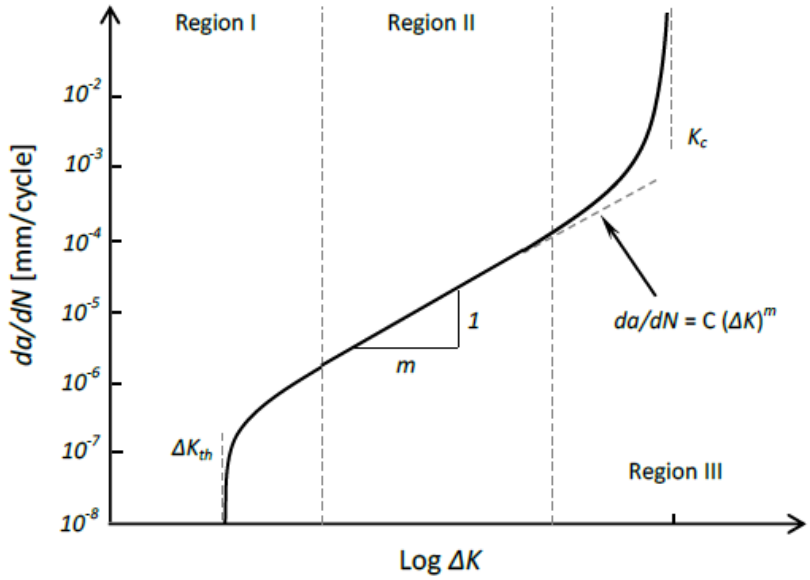

Figure 16. Fatigue crack propagation regimes [6].

The crack growth rates in multiaxial fatigue loading may be determined using an equivalent stress intensity range, ΔK_{eq}. The multiaxial fatigue evaluations are conducted with Paris simple power law by replacing ΔK_I with ΔK_{eq} [35,36]:

$$\Delta K_{eq} = \left[\Delta K_I^4 + 8 \cdot \Delta K_{II}^4 + \frac{8 \cdot \Delta K_{III}^4}{1-\nu}\right]^{0.25} \quad [35] \tag{2.52}$$

$$\Delta K_{eq} = [\Delta K_I^2 + \Delta K_{II}^2 + (1+\nu) \cdot \Delta K_{III}^2]^{0.5} \quad [36] \tag{2.53}$$

where ν is the Poisson's ratio.

The numerical automatic crack-box technique was developed to perform fine mixed-mode fracture mechanics calculations. This technique was proposed by Lebaillif et *al.* [37] and consists of the following steps:

i) Meshing of the three regions for the initial crack;

ii) Performing finite element method calculations associated with crack extension criterion in order to determine the crack extension angle;

iii) Taking a crack growth increment in the direction corresponding to the crack extension angle;

iv) Updating of local crack tip region mesh and connecting it by the use of transition zone to the whole structure.

Another technique based on a two-step approach [38,39] was proposed in order to compute the stress intensity factors of the mixed mode crack propagation tests using modified CT geometries. The experimental data assessment for the mixed mode tests is performed using Digital Image Correlation (DIC). DIC is used with two purposes:

i) Crack path evaluation;

ii) Stress intensity factors computation.

3. PROPOSED PROCEDURE FOR FATIGUE LIFE ESTIMATION OF HALF-PIPES BOLTED CONNECTION

The proposed procedure to multiaxial fatigue life estimation of steel half-pipes bolted connections applied in global structural models with beam elements using local approaches can be summarized as follows [40]:

i) Linear-elastic analysis of the global structural model using beam elements;

ii) Definition of the global/local interface with the critical region identification and interpolation region specification;

iii) Local model definition of the connection in order to build the local model using linear-elastic analysis to obtain the stiffness of the joint;

iv) An elastoplastic analysis of the local model is also required to determine the maximum principal stresses and strains at the fatigue critical points;

v) Local multiaxial fatigue damage analysis at the critical point using a multiaxial damage criterion.

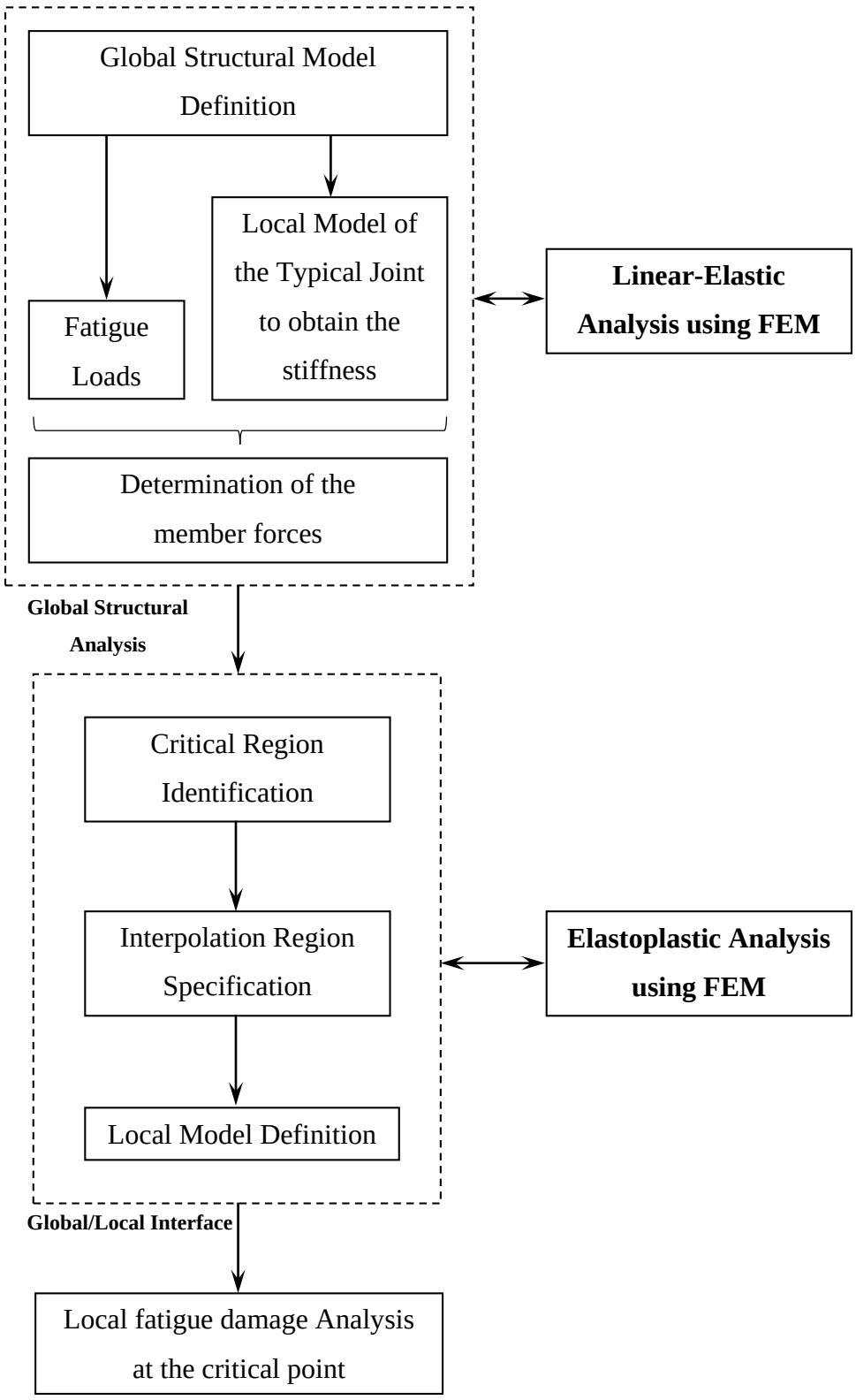

Figure 17. Schematic explanation of fatigue analysis procedure.

4. EXPERIMENTAL FATIGUE DATA OF THE S355 MILD STEEL

The fatigue behaviour of the S355 mid steel was evaluated by De Jesus et al. [41,42], based on experimental results from fatigue tests of smooth specimens and fatigue crack propagation tests.

The fatigue tests of smooth specimens were carried out according to the ASTME606 standard [43], under strain-controlled conditions. Tables 1 and 2 summarize the elastic (E: Young modulus) and monotonic strength properties (f_y: yield strength; f_u: tensile strength) as well as the cyclic elastoplastic constants (K': cyclic strain hardening coefficient; n': cyclic strain hardening exponent) and the strain-life constants (refer to Eq. (2.12)). Figure 18 illustrates the resulting experimental strain-life fatigue data.

The crack propagation tests were performed using compact tension (CT) specimens, according to the procedures of the ASTM E647 standard [44], under load-controlled conditions. Fig. 19 presents the experimental fatigue crack propagation rates obtained for the S355 steel, where stress ratio effects on fatigue crack propagation rates are shown. An increase in fatigue crack propagation rates is clear, when the stress ratio changes from 0 to any positive stress ratios considered in the experimental program. Also, it is clear that all the positive stress ratios resulted in similar crack propagation rates. This behaviour is consistent with a crack closure effect that occurs between R_σ=0.0 and R_σ=0.25. For R_σ=0.0 there is some crack closure, the applied stress intensity factor range being not fully effective. For R_σ=0.25 and higher, there is no crack closure, the applied stress intensity factor range being fully effective. Details about the properties evaluation for the S355 steel can be found in reference [41,42].

Table 1. Monotonic and cyclic elastoplastic properties of the S355 mid steel.

E	f_u	f_y	K'	n'
GPa	*MPa*	*MPa*	*MPa*	-
211.60	744.80	422.000	595.85	0.0757

Table 2. Morrow constants of the S355 mid steel.

σ'_f	b	ε'_f	c
MPa	-	-	-
952.20	-0.0890	0.7371	-0.6640

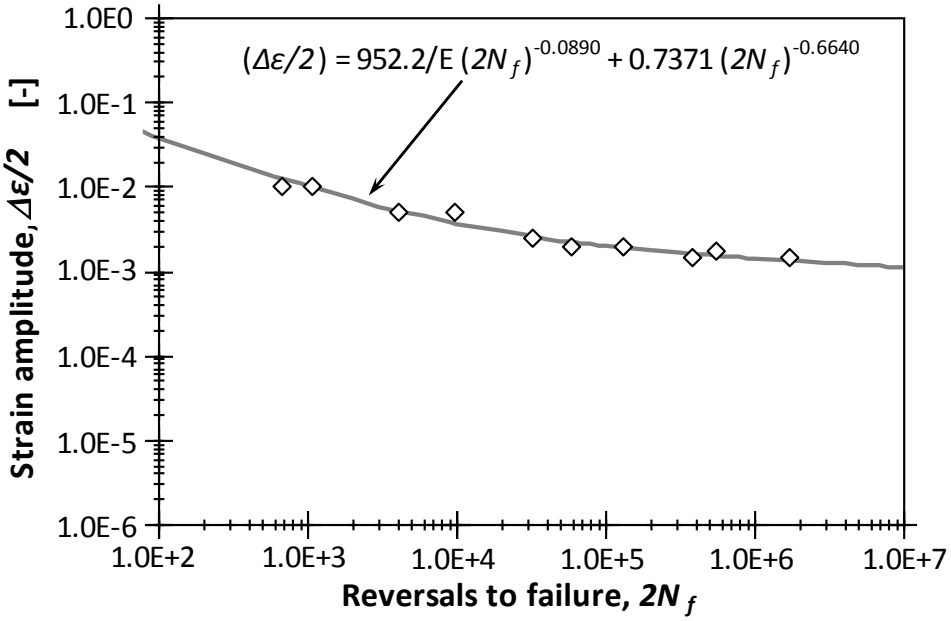

Figure 18. Strain-life curves for the S355 steel, R_ε=-1.

Basis of those results it is possible to get the *SWT* parameter based on *SWT-N* model proposed by Smith, Watson, and Topper [13]. Using this model and assuming that the *SWT* parameter corresponds to critical plan for the maximum stress, these experimental results are used to assess the multiaxial fatigue.

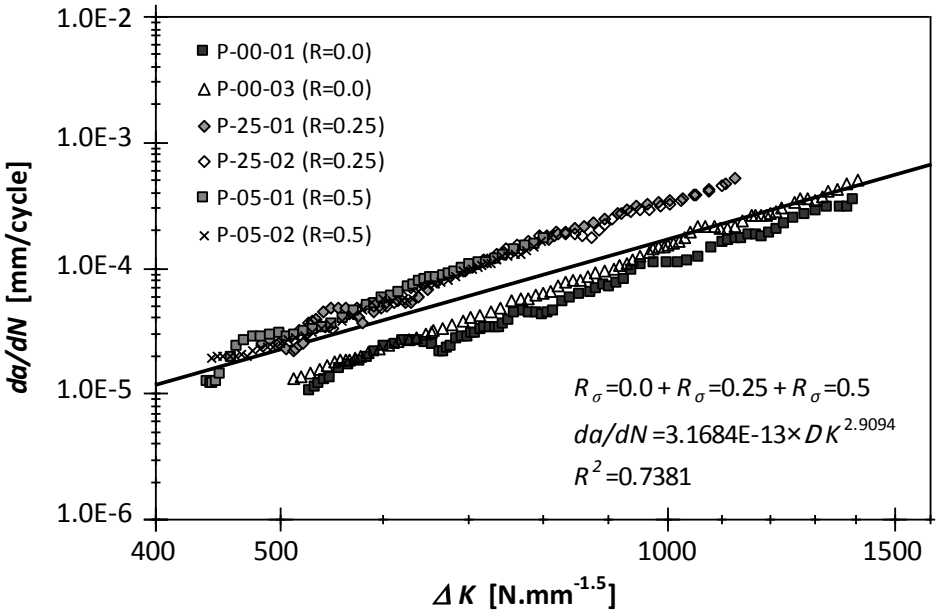

a) Experimental data

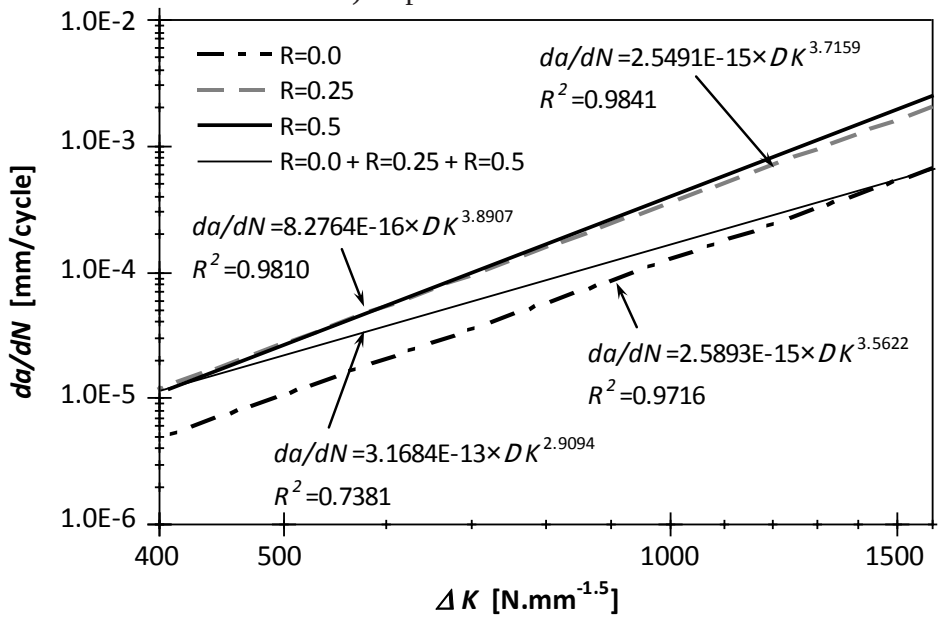

b) Paris correlations for each stress R_σ-ratio

Figure 19. Experimental fatigue crack propagation data of the S355 steel for distinct stress ratios: experimental results [41,42].

5. NUMERICAL MODELLING

In this work, numerical modelling of tubular bolted connection of a lattice tower for wind energy converters was done in order to assess fatigue life behaviour. The procedure adopted for fatigue evaluation is proposed in chapter 3. The series of work performed in this chapter is given below in detail.

5.1 Numerical Modelling for fatigue assessment

Numerical modelling of steel structures for fatigue assessment is an advanced yet necessary tool due to the complex geometries, therefore, stress and strain distributions. In order to estimate the fatigue strength of the bolted joint, the distribution of stress and strain should be obtained around the bolt hole, and finally, the number of cycles to failure can be calculated from selected fatigue criteria. To do so, a 3D finite element analysis was performed using ABAQUS 6.14-2 [45] finite element code in order to obtain the stress and strain distribution in the members of tubular bolted connection of wind turbine lattice tower.

Numerical modelling of the joint for fatigue assessment have been completed in three main steps:

i) stiffness analysis of the joint;

ii) application of joint stiffness to general beam model to obtain realistic member forces;

iii) analysis of the joint under applied member forces.

Analysis of the joint is composed of two main steps:

i) Applying preload to bolts;

ii) External loading of the joint in members.

A special feature of Abaqus/Standard solver was used for preloading by applying a shortening to the middle section of bolts. A preliminary analysis to define correct preload of bolts was also performed before analysing the stiffness of the connection.

5.2 Simple model to define bolt pre-loading

Calculation of preload according to EN 1993-1-8 [46] was made and in order to obtain correct value in analysis result, a simple preloading model was investigated (Figure 20). An approximate value of strain loading to bolt cross section was applied according to the following calculation;

$$F_{P,cd} = 0.7 * f_{ub} * \frac{A_s}{\gamma_{M7}} = 0.7 * 1000 * \frac{561}{1.1} = 357\ kN$$

$$\sigma = \frac{F}{A} = \frac{357000}{561} = 636.364\ \mathrm{N/mm^2}\ , \qquad \epsilon = \frac{\sigma}{E} = \frac{636.364}{210000} = 0.00303$$

$$\Delta l_1 = \epsilon * L_1 = 0.00303 * 94 = 0.285\ mm$$

and increased to 0.358 mm to obtain the correct force value in the bolt section.

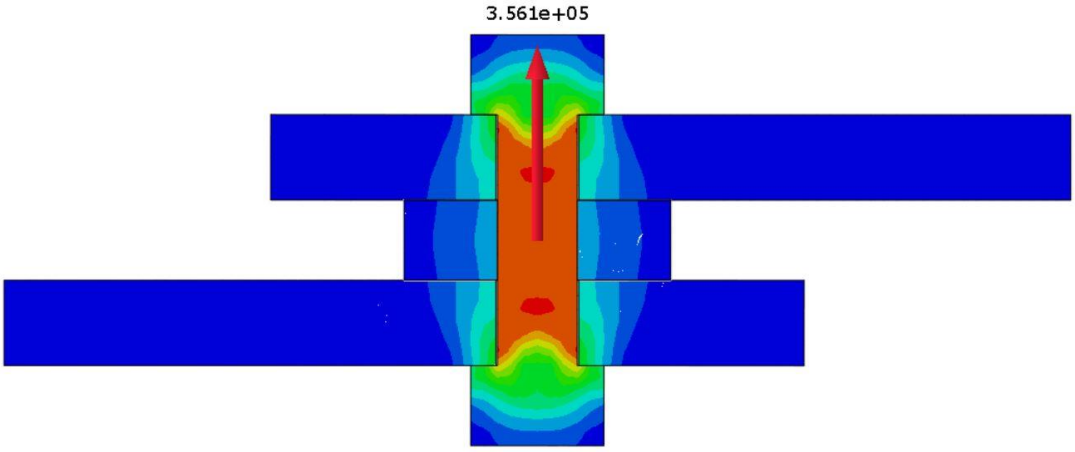

Figure 20. Preload validation (356.1 kN).

5.3 Stiffness model

In this chapter, as the first step of the numerical part, a 3D finite element model developed in order to help calculate stiffness of the joint as shown in Figure 21. As a simplification, only one half of the KK joint has been modelled. Elastic material behaviour, E=210GPa and poisson ratio 0.3 were used.

Finite element model is composed of nearly 40.000 quadratic C3D20R and 250.000 linear C3D8R elements for gusset plates and other parts respectively. Element size varies between 10 mm and 50 mm depending on the location, smaller elements around bolt holes and bigger elements in other parts. To extract more accurate results, mapped mesh with sufficiently fine

mesh around the hole of the plates has been used in FE analyses. The friction effect between the surfaces of the bolt head and plates was included in the FE model using Elastic Coulomb model with friction coefficient of 0.35 which is an average value of what has been used in some previous studies

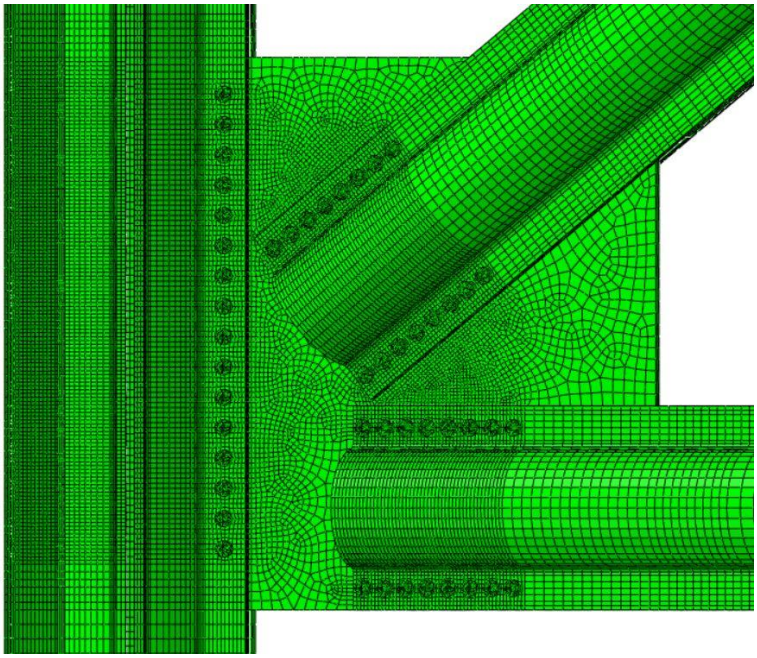

Figure 21. Stiffness model.

5.4 Approach to obtain stiffness of the joint

A simple hand calculation was made by finding relation between rotation and force according to result obtained in stiffness model analysis. Figure 22 represents the stiffness calculation method where F is applied force, a is distance to centre of bolt group, Δ is displacement of centre of bolt group, ϕ is rotation of member and l is distance to the axis of chord from centre of bolt group:

$$\frac{\Delta}{l} = \emptyset \tag{5.1}$$

$$F.a = M \tag{5.2}$$

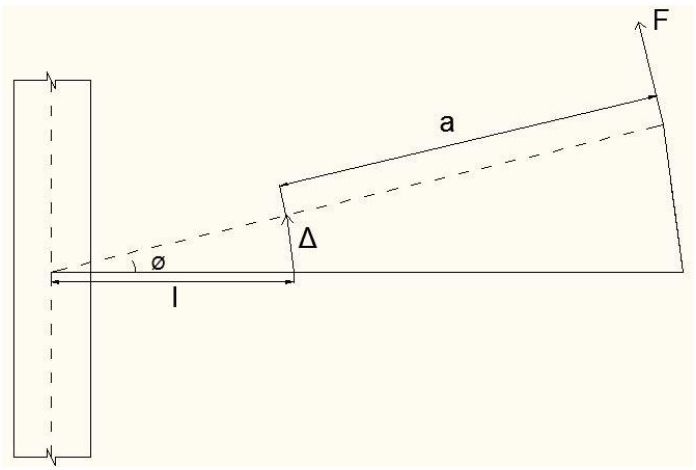

Figure 22. Stiffness calculation.

Following the simple method above, stiffness of the joint was calculated for three different models using C3D20R, C3D10 and C3D10M with second order accuracy elements for gusset and C3D8R for other parts. Moment rotation relation of these models is shown in Figure 23. Result of the model with C3D20R was used and is suggested because of the computational time required and the stress results.

According to the simple calculation method described above, rotational stiffness of the joint is found to be 3.73kNm/rad.

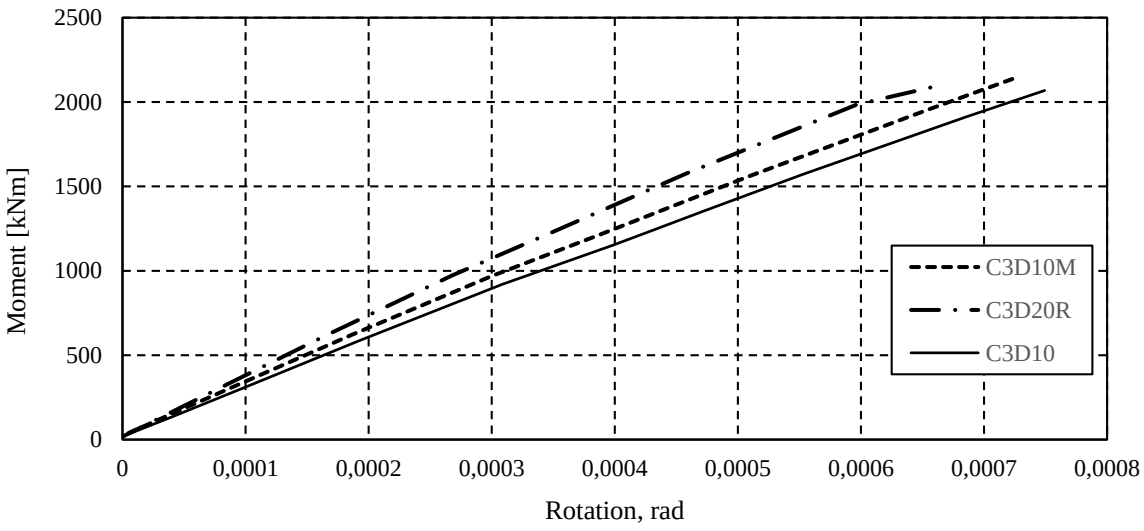

Figure 23. Elastic joint stiffness.

5.5 Global modelling with beam elements to obtain realistic member forces

5.5.1 A simple model for the verification of connector element

Joints in truss structures are usually considered as pinned for the simplicity. However, in reality these bolted joints in such a case should be considered as semi-rigid, therefor, they should be represented by defining rotational stiffness. To this end, "Join+Rotation" type of connector element was used to represent the semi-rigid joint stiffness. Verification of the simple model was done by applying 1 kN point load on a beam with length of 100 mm and a rotation stiffness of 1000000 Nm (Figure 24). Simple calculation of moment-rotation behaviour is done as follows:

$$M = k \cdot \theta \tag{5.3}$$

By using the values given in Figure 24, and using the Equation 5.3,

$$1000 \cdot 100 = 1000000 \cdot \left(\frac{10}{100}\right)$$

It is possible to prove that "Join+Rotation" connector works correctly for the purpose.

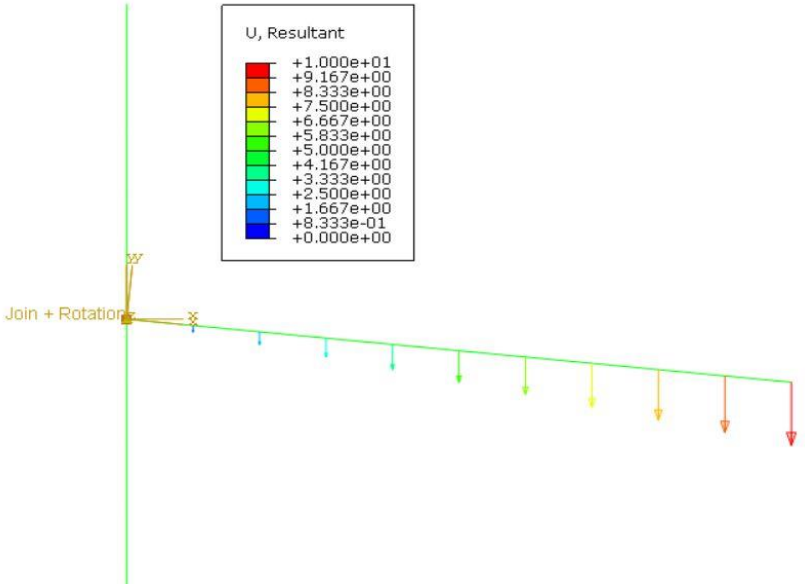

Figure 24. Connector element used for stiffness.

5.5.2 Global model with beam elements

Global model of lattice tower structure is composed of 8 chord members with a length of 54.83 m placed with an angle of 66° resulting in a lattice tower height of approximately 50 m, 64 braces and 72 horizontal members whose dimensions are given in Table 3.

Global analysis of lattice tower was also carried out in Abaqus 6.14 [45] using beam elements to have results in a reasonable computational time. A 3D model with beam elements combined with the calculated joint stiffness in the previous section have been used for global analysis of the lattice tower in order to obtain member forces (Figure 25). As the nature of this analysis is elastic only young modulus of 210GPa and poisson ratio of 0.3 were defined in material properties.

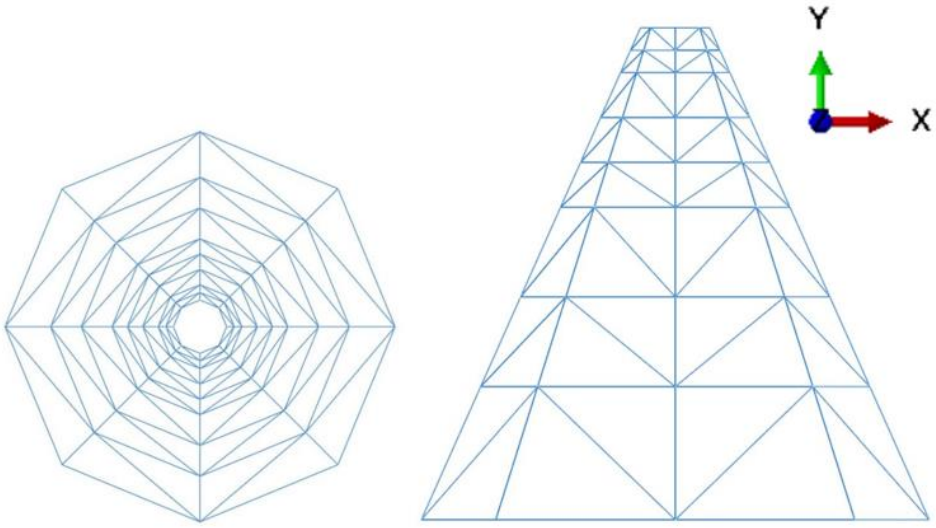

Figure 25. Global model.

Table 3. Dimensions of structural members in lattice tower.

Level	*Member length (m)*		
	Chords	*Horizontal members*	*Braces*
Top	0	2.7	0
7	2.5	3.48	3.95
6	2.5	4.26	4.59
5	5	5.81	7.05
4	5	7.37	8.24
3	5	8.93	5.28
2	10	12.0	14.4
1	10	15.15	16.8
Bottom	14.83	19.77	22.78

Boundary conditions of lattice tower applied directly to bottom nodes. Bottom nodes of the lattice tower restrained in all translational directions while their rotations kept free. Moreover, loads were applied through a reference point at the centre of top octagon.

Global model was analysed under fatigue load conditions obtained in previous studies [47]. Damage equivalent fatigue loads used in the analysis are shown in Table 4. In order to show the effect of semi-rigid connection modelling a comparison was made between the results for pinned, semi-rigid and rigid connections. According to the modelling procedure explained above member forces shown in Table 5 obtained in the global analysis (Figure 26).

Table 4. Damage equivalent fatigue loads applied in global beam model.

ΔFx (kN)	*ΔMx (kNm)*	*ΔMy (kNm)*	*ΔMz (kNm)*
203	781	4065	3950

Table 5. Member forces obtained in global analysis.

Member name	***Pinned***		***Semi-rigid***			***Rigid***		
	Fx (kN)	***Fy (kN)***	***Fx (kN)***	***Fy (kN)***	***Mz (kNm)***	***Fx (kN)***	***Fy (kN)***	***Mz (kNm)***
Horizontal-1	-231.02	0	-227.117	13.62	0.04	-210	9.93	16.4
Brace-1	231.02	215.33	319.088	1.38	0.547	307.274	178.15	5.7
Brace-2	-167.37	207.7	-315.981	3.9	0.487	-302.74	175.79	-5.57
Horizontal-2	140.615	0	218.185	-14.38	0.084	300.59	9.06	-14.66

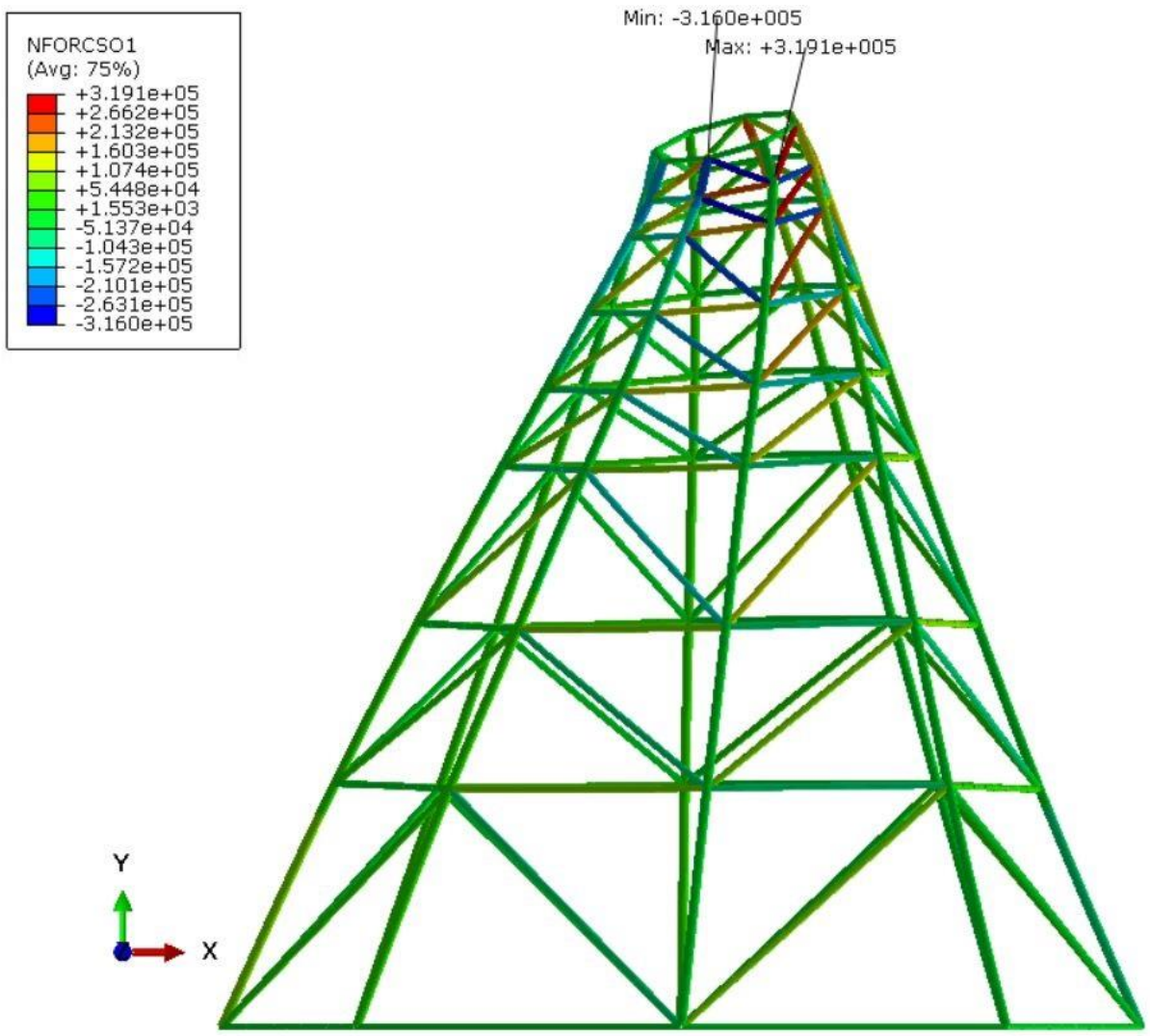

Figure 26. Max. and min. axial forces in members.

5.6 Application of Obtained Member Forces to Joint Model

5.6.1 Geometric properties of the model

Abaqus 6.14 [45] model of tubular bolted connection of the lattice tower under investigation is given in Figure 27. Numerical model is composed of chord, horizontal and diagonal members which are connected by gusset and filler plates. Cross-section and members length used in the analysis is given in Table 6.

Table 6. Cross-section properties of members

Member	Cross-section	Length
Chords	CHS 559 x 32 mm	6000 mm
Braces	CHS 406.4 x 32 mm	5000 mm
Horizontal bars	CHS 406.4 x 32 mm	5000 mm

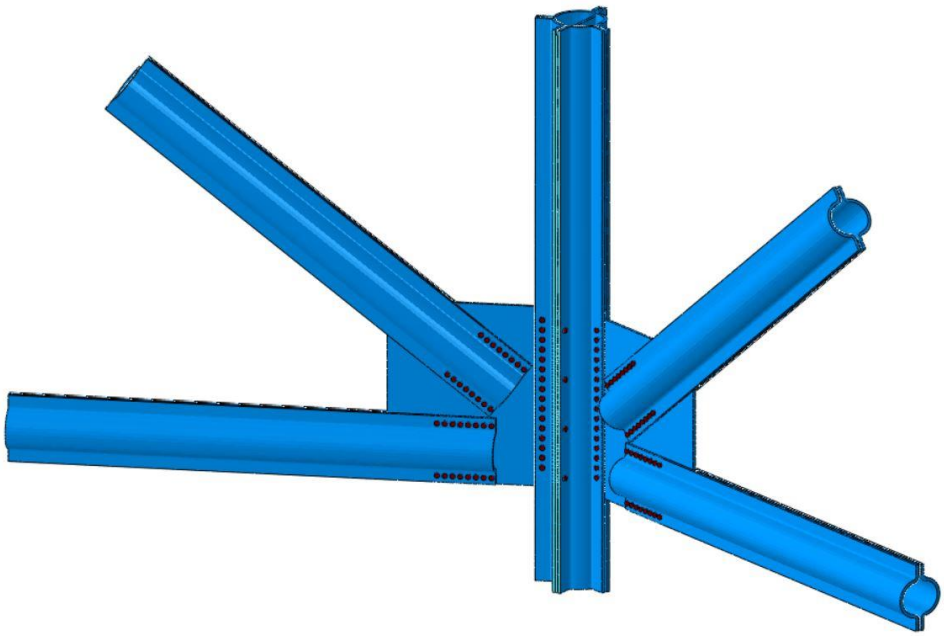

(a)

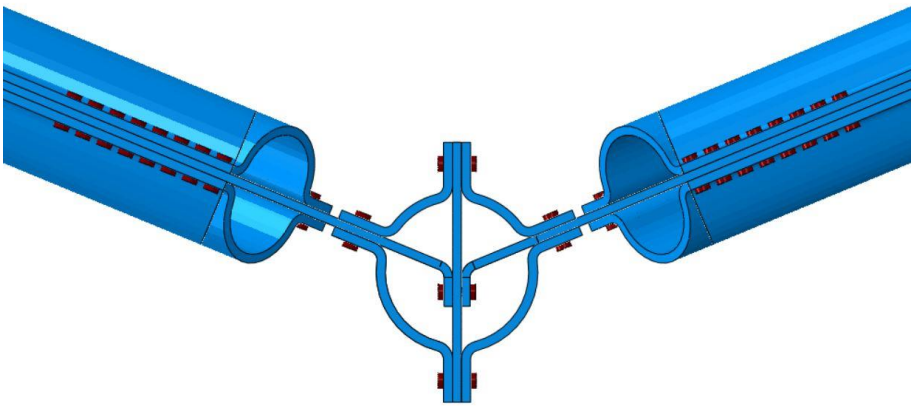

(b)

Figure 27. 3D and cross-section views of the bolted joint.

5.6.2 Material, element type and mesh

Most materials that exhibit ductile behaviour (large inelastic strains) yield at stress levels that are orders of magnitude less than the elastic modulus of the material, which implies that the relevant stress and strain measures are "true" stress and logarithmic strain. Material data for all of these models should, therefore, be given in these measures. Conversion of nominal stress-strain data is performed as follows:

$$\varepsilon_{ln}^{pl} = \ln(1 + \varepsilon_{nom}) - \frac{\sigma_{true}}{E} \tag{5.4}$$

$$\sigma_{true} = \sigma_{nom}(1 + \varepsilon_{nom}) \tag{5.5}$$

The elastoplastic monotonic behaviour of S355 steel grade used in this study is shown in Figure 28 below. This material data were taken from a previous study performed by De Jesus et *al.* [41,42]. Bolts were assumed to have a linear elastic material relationship with a Poisson ratio equal to 0.3 and young modulus of 210GPa. As the bolt and its washer have approximately the same material properties, the geometrical model of the washer was added to the bolt head in order to minimize the interaction use (with ignoring contact definition between the bolt head and the washer). This simplification considerably reduces computation processing time with very good approximation.

Isotropic hardening is used for the material that allows yield surface to change size uniformly in all directions such that the yield stress increase (or decrease) in all stress directions as plastic straining occurs. Fatigue data for the S355 steel used in this study, are presented in the Chapter 4. Theses cyclic properties of the S355 steel were used for fatigue assessment of the joint in study.

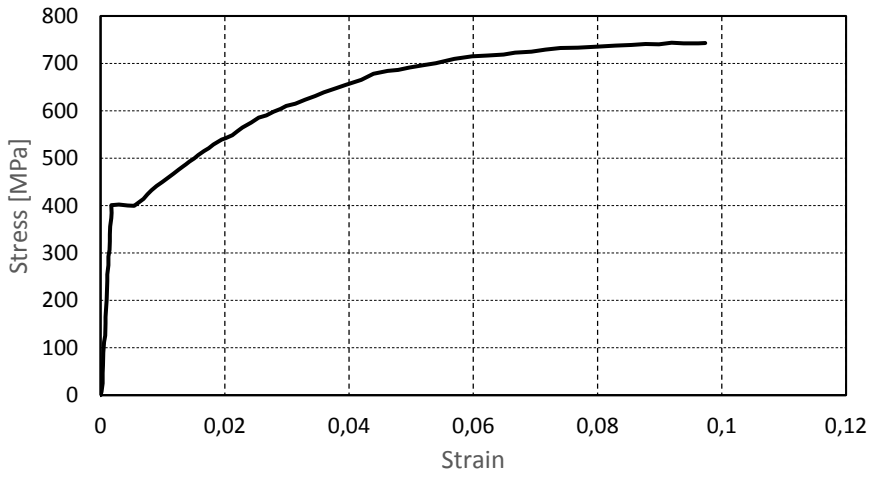

Figure 28. Monotonic behaviour of the S355 steel used in this study.

A mesh convergence study was carried out on a double lap joint representing two horizontal members and gusset plate connection using same thickness and bolt diameter in order to obtain an optimum solution between result accuracy and computational time. Mesh convergence criteria was considered to be 5 % difference from previous analysis in maximum stress under preloading of bolt.

Figures 29 and 30, and Table 7 show variation of number of elements around bolt holes and through thickness used in the convergence study and the results respectively. As it can be seen from Table 7, using 4 elements through thickness with variation of (6, 5, 8) elements on edges a, b and c satisfy the convergence criteria. Moreover, minimum element size is 2.9 mm in this preference.

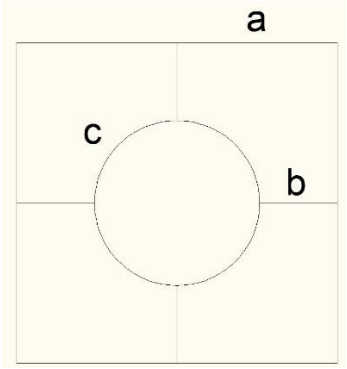

Figure 29. Number of elements used around bolt holes.

Table 7. Analyses performed for mesh convergence study

Analysis number	*Through thickness*	*a*	*b*	*c*	*Maximum stress*	*Difference (%)*
1	3	6	5	8	325.5	-
2	4	6	5	8	350.7	7.75
3	5	6	5	8	367.8	4.8
4	6	6	5	8	384.47	3.5
5	4	4	3	6	279.3	-
6	4	4	4	6	311.2	11.4
2	4	6	5	8	350.7	12.6
7	4	6	5	10	340.3	3

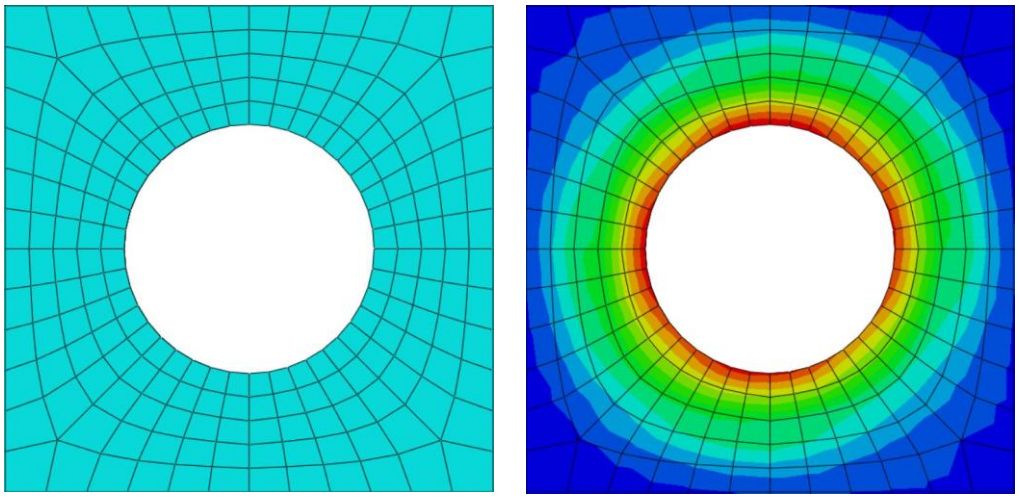

Figure 30. Number of elements used around bolt holes and stress distribution after preloading.

Two different meshing approaches were used in this study namely top-down and bottom-up for chord, braces, horizontal members and gusset plates respectively due to irregular shape of gusset plate. Structured mesh was applied to regions around bolt holes in order to obtain a well distributed stress, therefor better results. All members in the joint consist of approximately 915.000 C3D8R, three dimensional solid elements with reduced integration points and hourglass control option. Also, using 4 elements through thickness in gusset plates, chord, braces and horizontal members is a good enough attempt to avoid hourglass effect. Some members and their mesh structures are also shown in Figure 31.

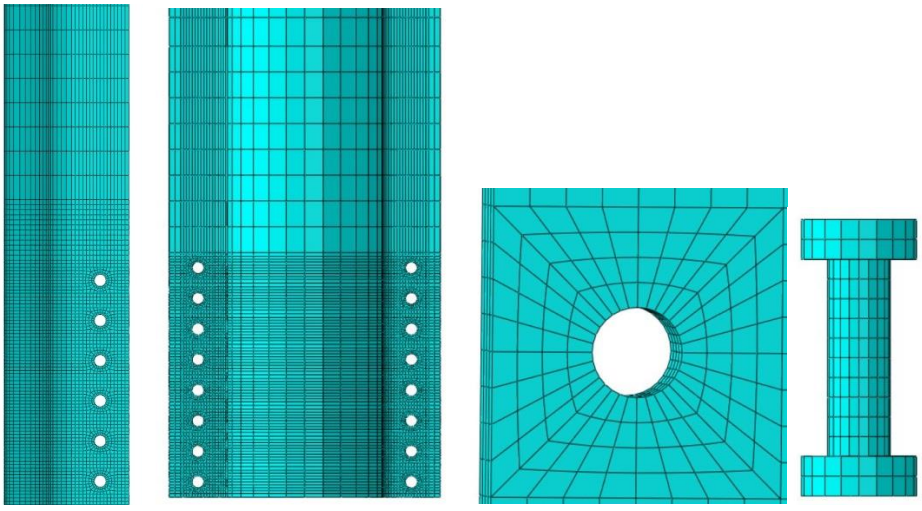

Figure 31. Mesh structure of some members.

5.6.3 Interaction definitions

Penalty friction formulation with an isotropic friction coefficient of 0.35 as tangential behaviour and hard contact which also allows separation after contact for normal behaviour were used. Surface-to-surface contact type with finite sliding with automatic surface smoothing option was used for contact definitions where adjustment of slave surfaces to remove overclosure option also chosen for members initially in contact.

Bolts were always chosen as master surfaces where members with more mesh density were chosen as slave surfaces. In order to help decrease computational time filler plates tied to braces, chords and horizontal members in a manner with minimally affecting the regions connected by bolts.

Table 8. Comparison between penalty and augmented Lagrange formulations

Augmented Lagrange			***Penalty***	
Stiffness	***Penetration tolerance***	***Max. stress***	***Stiffness***	***Max. stress***
default	default	245.2	default	220.5
100	default	230.4	100	561.4
10	default	317.2	10	476.5
1	default	-	1	296.4
default	1	245.2	0.1	-
default	0.1	245.2	-	-
default	0.01	245.2	-	-

A parametric study was also performed to decide between penalty and augmented Lagrange contact formulations taking into account maximum stress and analysis time. As it can be seen in Table 8, the stiffness of the contact significantly affects the maximum stress occurring in a contact area and keeping contact stiffness same and varying the penetration tolerance in augmented Lagrange formulation shows that this variable has no effect on the maximum stress.

Moreover, increasing the contact stiffness also increased the computational time at an exponential rate and lowering stiffness resulted in not converging solutions. Dashed cells in the Table 8 indicate that analysis did not converge. Judging by the parametric study performed on contact formulations above it was decided to use penalty contact formulation with default values.

5.6.4 Boundary conditions

In loading step all horizontal members and braces restrained in out of plane direction and left free to move in other directions (u_x=0, u_y=u_z≠0) while bottom and top cross sections of chord

were restrained in all directions (u_x=u_y=u_z=0) by means of coupling all the nodes on end cross sections of members to reference points.

5.7 Numerical results

The proposed procedure to multiaxial fatigue life estimation of steel tubular bolted connections applied in global structural models with beam elements using local approaches is presented in Chapter 3.

Table 9 shows stress, strain and *SWT* parameter results obtained at the end of external loading. As it can be seen from the table maximum *SWT* resultant occurs in Horizontal-8 although resultant *SWT* parameters have almost no difference from one another. This is due to the fact that preloading of bolts has significant effect compared to external loading which resulted from fatigue equivalent loads (see Figure 32).

Figure 33 and Fig 34 also show von misses and maximum principal stress distributions respectively.

Table 9. Maximum stress (in MPa), strains and *SWT* parameters in members.

S11	***S22***	***S33***	***E11***	***E22***	***E33***	$\varepsilon_a.\sigma_{max}$	***Part***
413,8270	43,5495	166,1310	0,0017	0,0006	0,0001	0,3492	Horizontal-1
415,7370	76,2876	140,5830	0,0017	0,0004	0,0001	0,3476	Horizontal-2
412,671	41,282	157,082	0,00169	0,000617	0,000102	0,3486	Horizontal-3
413,782	42,12	164,024	0,001686	0,000625	0,00013	0,3487	Horizontal-4
415,368	49,9184	164,558	0,00168	0,000606	0,000127	0,3490	Horizontal-5
413,91	42,3622	165,166	0,001687	0,000637	0,000144	0,3491	Horizontal-6
413,145	42,9085	160,734	0,001693	0,000627	0,000123	0,3497	Horizontal-7
414,967	42,203	166,237	0,001696	0,00064	0,000146	0,3520	Horizontal-8
246,7700	106,3200	34,6455	0,0010	0,0001	0,0003	0,1201	Gusset-1
104,2580	15,3508	1,7635	0,0005	0,0001	0,0002	0,025017	Gusset-2

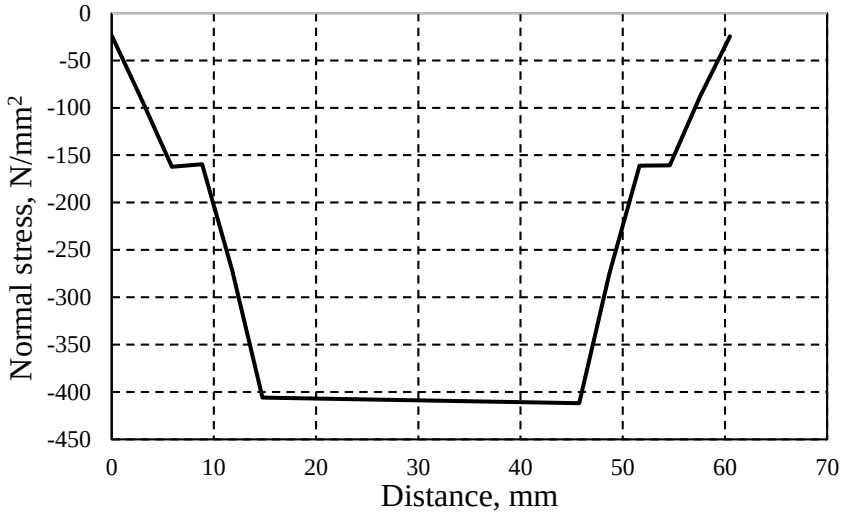

(a)

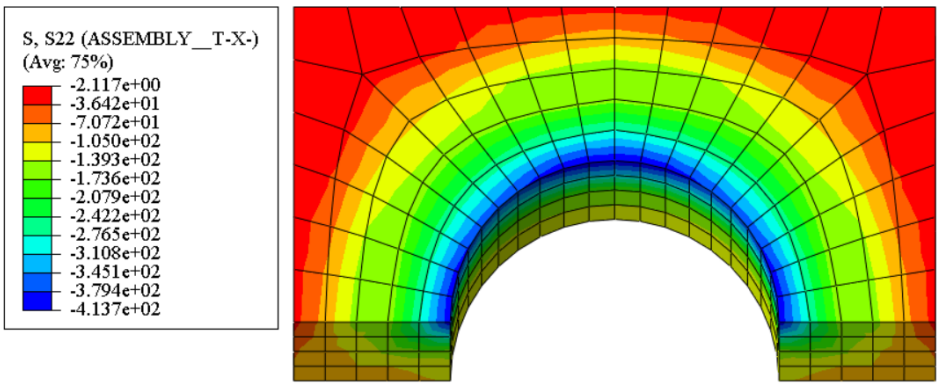

(b)

Figure 32. Normal stress due to bolt preloading; (a) by distance, (b) by contour.

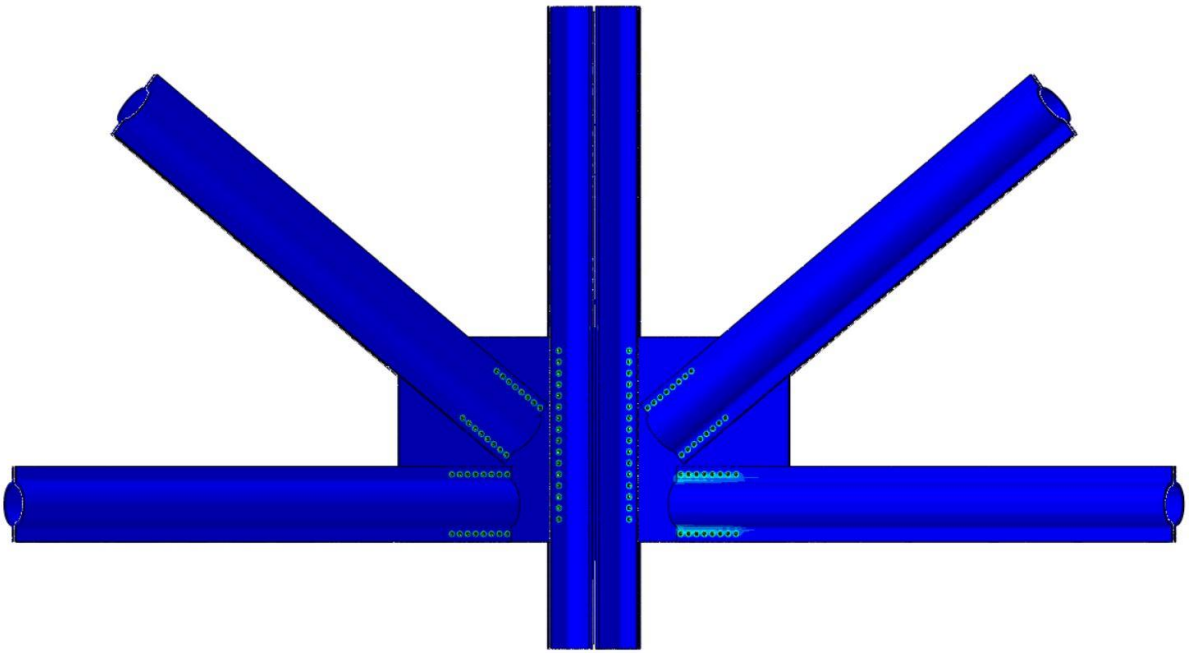

Figure 33. Von-misses stress distribution due to external loading.

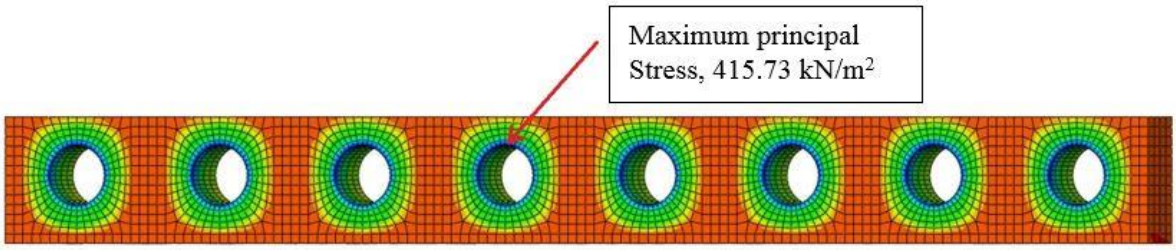

Figure 34. Maximum principal stress location.

Figure 35 shows *SWT* resultant variation according to bolt force during preloading and external loading. Application of external loads resulted in hardly any change in bolt force. Therefore, preload of bolts is considered to be the governing factor for fatigue life estimation of tubular bolted connection under investigation as no change was observed in *SWT* resultant during external loading.

Figure 36 shows *SWT* parameter-fatigue life variation of unnotched specimen of S355 mild steel. According to the multiaxial fatigue criterion, which was used in this study, namely Smith-Watson-Topper criterion [13], the resultant parameter was calculated as 0.352 which gives the fatigue life N_f approximately 815.000 cycles.

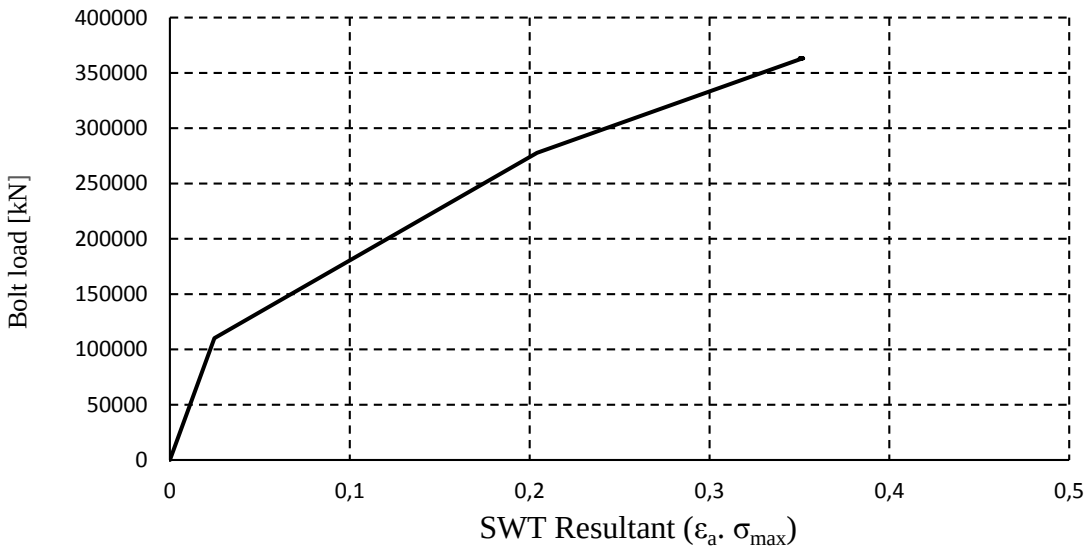

Figure 35. *SWT* resultant variation to bolt load.

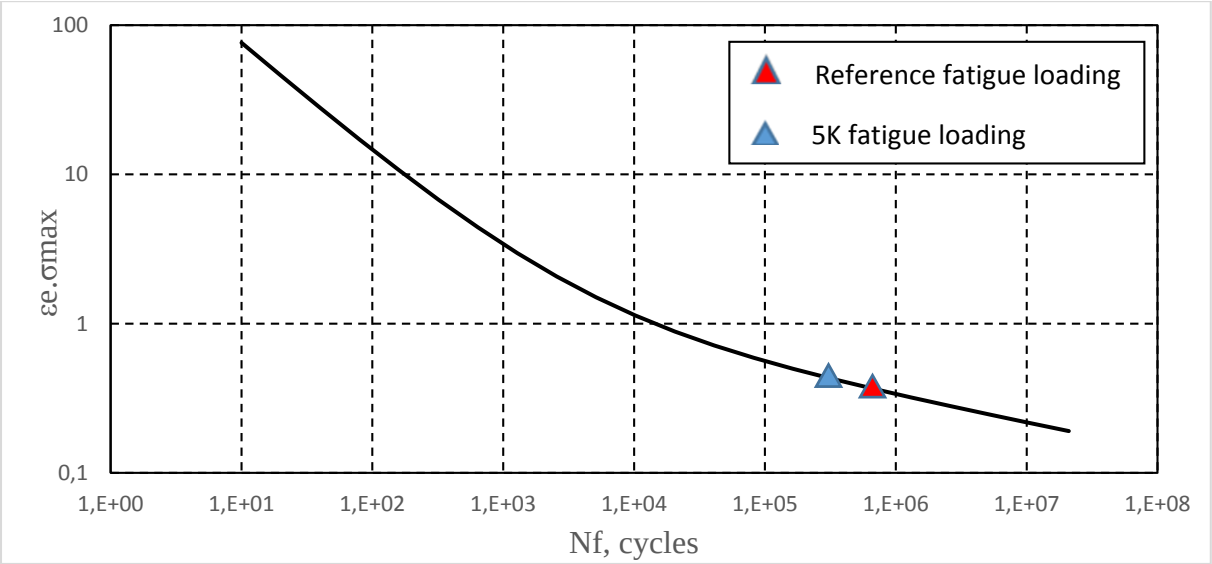

Figure 36. *SWT* resultant fatigue life curve for the S355 steel unnotched specimen.

Fatigue life behaviour of the tubular bolted connection was also further investigated under up to five times the reference equivalent fatigue loads (5K). Figure 37 shows variation of maximum principal stresses at minimum fatigue life location on Horizantal-8 member under 5K loads. Initial stress increase represents preloading stage of the analysis and the rest shows external loading. It is important to note that even though 5K loads were applied in this case, the change in local stress variation was observed to be around 3% which can be considered ineffective for such amount of increase in loading. It can then clearly be concluded from the figure that local stresses in any direction did not change up to 5K external loading.

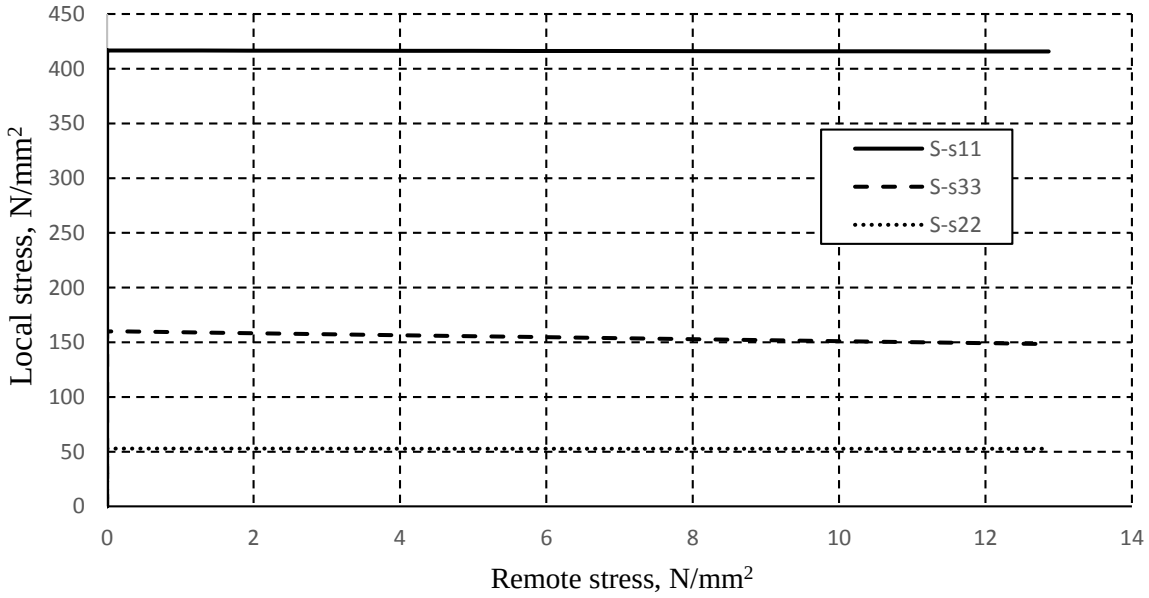

Figure 37. Remote stress-local stress (5K) variation at minimum fatigue life location.

Figure 38 shows *SWT* parameter variation from preloading until the end of external loading in time. It should be considered that preloading ends at the end of one second and external loading starts at this point. Addition to Figure 37, Figure 38 also indicates very little effect of 5K external loading on *SWT* parameter, therefore, little or no change in fatigue life can be expected.

However, it is important to note that 3% increase in the *SWT* parameter from K to 5K loading resulted in a fatigue life of 630000 cycles which corresponds to a decrease of 23% in fatigue life compared to 815000 cycles of N_f in K loading.

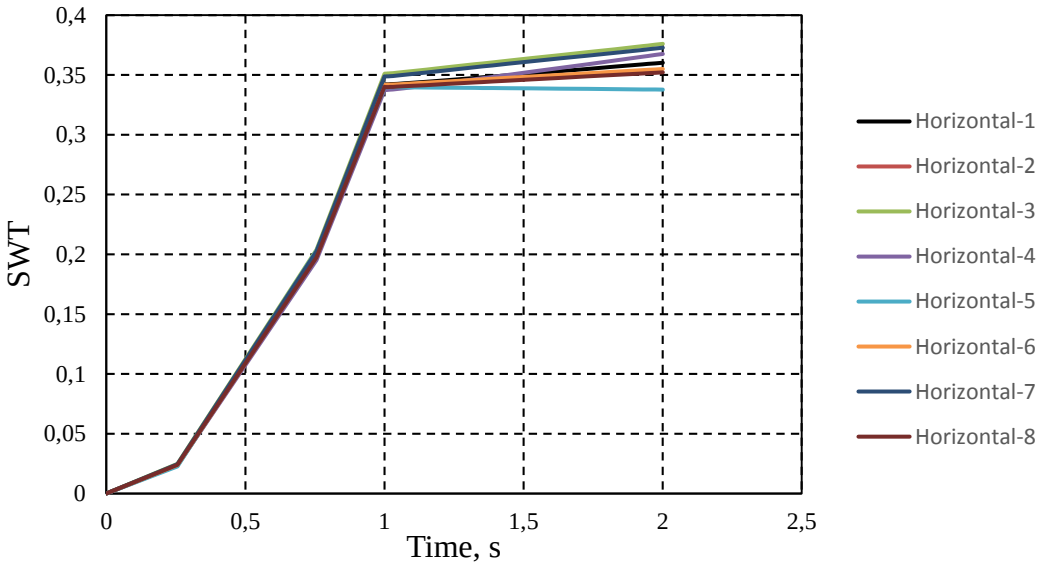

Figure 38. S*WT* parameter variation.

Figure 39 shows stress gradient of cross-section where the minimum fatigue life occurs. It also shows the importance of relation between stress concentration around bolt holes and remote stress. Furthermore, Figure 40 and Figure 41 show stress gradient and stress integration respectively around the bolt hole with the finest mesh. This curves are important in terms of stress concentration factor calculations which can easily be defined and the ratio between nominal and maximum stress.

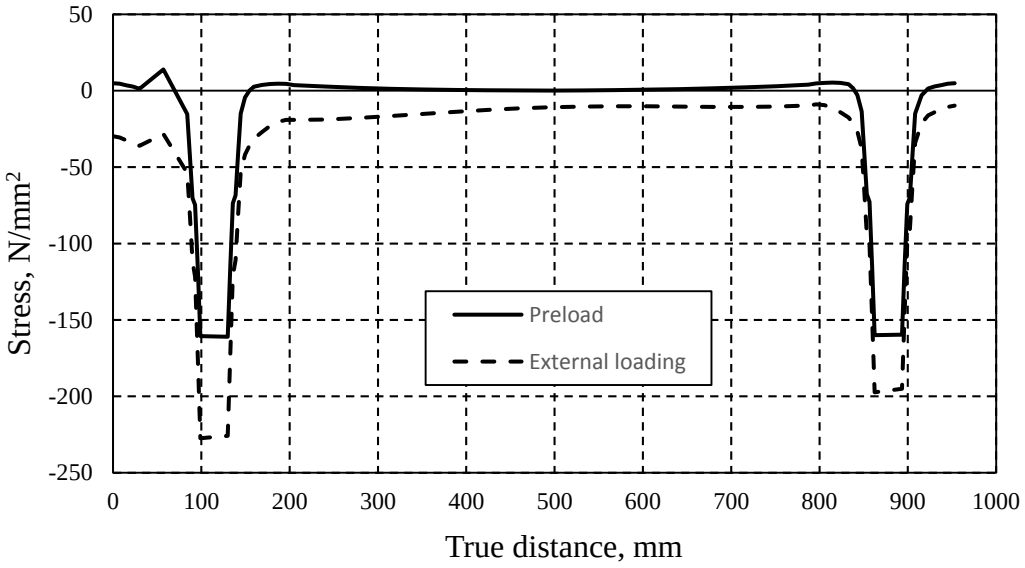

Figure 39. Shows stress gradient around bolt hole.

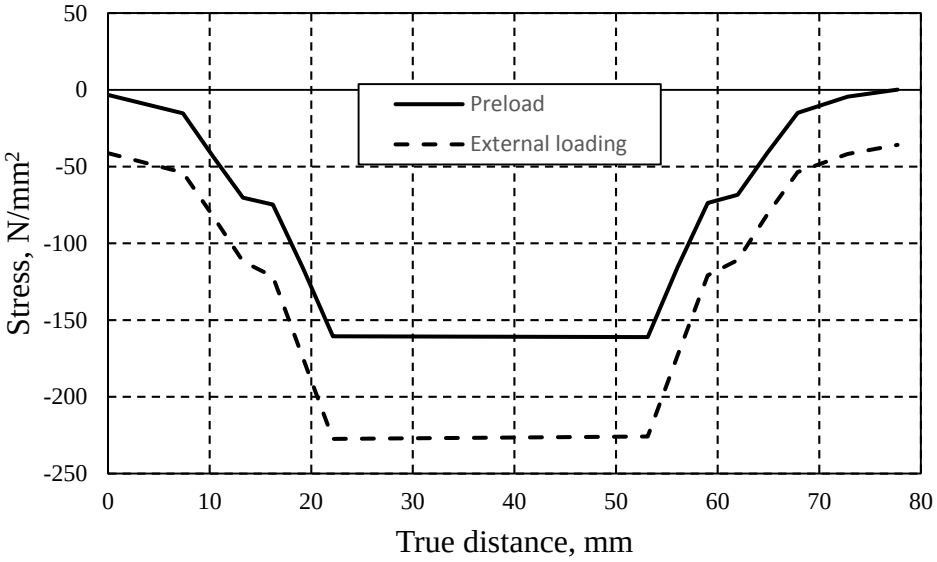

Figure 40. Shows stress gradient around bolt hole.

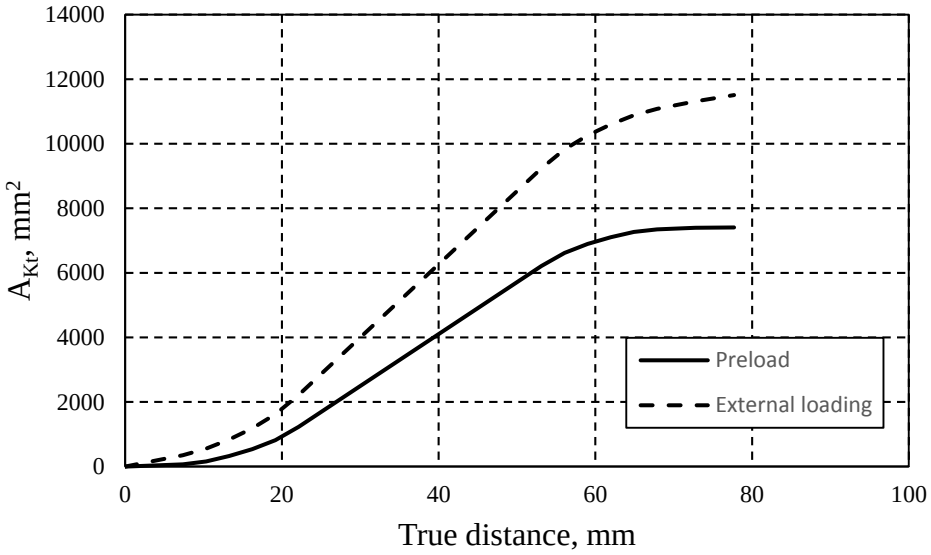

Figure 41. Integration of stress around bolt hole.

FEA results (path operations and integration to determine the area under the stress gradient curve) provides an accurate method of determining the nominal stress (σ_{nom}).

$$\sigma_{nom} = \frac{A_{Kt}}{Distance} = \frac{7279{,}95}{77{,}697} = 95{,}328 \frac{N}{mm^2}$$

$$where\ \ \sigma_{max} = 161{,}04\ \frac{N}{mm^2}\ (Preloading)$$

$$\sigma_{nom} = \frac{A_{Kt}}{Distance} = \frac{11505{,}1}{77{,}697} = 148{,}078\frac{N}{mm^2}$$

$$where\ \ \sigma_{max} = 227{,}45\ \frac{N}{mm^2}\ (External)$$

$$K_{t,Preload} = \frac{161{,}04}{95{,}328} = 1{,}689 \quad and \quad K_{t,External} = \frac{227{,}45}{148{,}078} = 1{,}536$$

Figure 42 shows gap size change between bolt and gusset plate hole. It can be seen from the figure that fatigue loads are not enough to cause a slippage greater than the size of the gap which prevents mechanical failure of gusset plate.

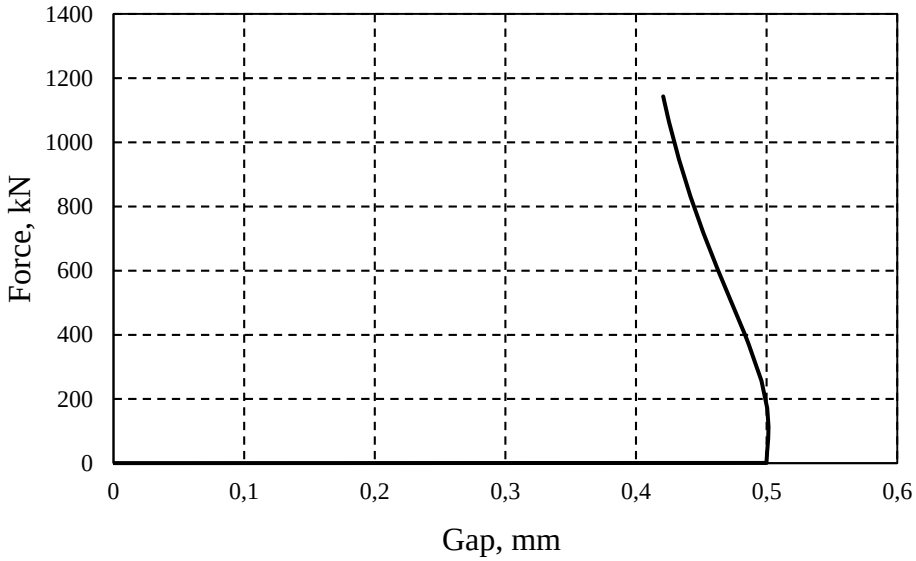

Figure 42. Gap size change between bolt and hole.

6. CONCLUSIONS AND FUTURE WORK

The purpose of this study was to investigate the fatigue life behaviour of tubular bolted connection of a newly proposed lattice tower using a multiaxial fatigue criteria. According to the work performed below conclusions can be drawn:

a) Rotational stiffness of the connection around the axis perpendicular to in-plane is found to be 3.6 kNm/rad;

b) Global model was analysed for pinned, semi-rigid and rigid connection cases and the axial forces difference in members between pinned and semi-rigid cases is found to be maximum up to 88 %;

c) Performing a mesh convergence study for preloading proved its importance as it has direct effect on fatigue life calculations;

d) Applied fatigue loads are not enough to cause important slippage of brace members on gusset plates which prevents mechanical failure of gusset plates as no interaction occurs between gusset plate hole and bolt. This stick regime suggest that the most possible fatigue failure location is under bolts in horizontal members and it should occur in form of wear failure which can be said to have longer fatigue life compared to mechanical failure,

e) No plastic strain observed due to preloading which causes the maximum stress,

f) In fatigue life calculations maximum resultant of *SWT* parameter was calculated for each member;

g) In every member, normal stress due to preloading was always the highest among other principal stresses;

h) All members were also loaded up to 5 times the reference equivalent fatigue loads to investigate further the fatigue life of members;

i) Increasing loads 5 times showed approximately 3% difference on normal stress but a 23 % decrease in fatigue life where it changed from 815000 cycles to 630000 cycles;

j) Stress concentration factors around bolt holes were calculated in the location with the minimum fatigue life as 1.689 and 1.536 for preloading and external loading respectively.

Some suggestion can also be made in order to improve the fatigue life calculations of tubular bolted connection under investigation such as: to perform stiffness calculation analysis for out-of-plane, improving rotational stiffness calculation method and including principal stress and strains in other directions then only normal direction in *SWT* parameter calculations which only considers the maximum principal stresses and strains. The use of the *SWT* parameter as a multiaxial damage criterion proved to be efficient in getting of the fatigue life of the steel half-pipe bolted connection.

REFERENCES

[1] Erich Hau, Wind Turbines Fundamentals, Technologies, Application, Economics, Third edition. Springer, 2012.

[2] Staffan Engström, Tomas Lyrner, Manouchehr Hassanzadeh, Thomas Stalin and John Johansson, Tall towers for large wind turbines Report from Vindforsk project V-342 Höga torn för vindkraftverk. 2010.

[3] Ralph I. Stephens, Ali Fatemi, Robert R. Stephens, Henry O. Fuchs, Metal fatigue in engineering, 2nd edition. Wiley, 2001.

[4] Jaap Schijve, Fatigue of structures and materials, Kluwer Academic Publishers, 2001.

[5] S. Bhat and R. Patibandla (2011). Metal Fatigue and Basic Theoretical Models: A Review, Alloy Steel - Properties and Use, Dr. Eduardo Valencia Morales (Ed.), ISBN: 978-953-307-484-9, InTech.

[6] José António Fonseca de Oliveira Correia, An Integral Probabilistic Approach for Fatigue Lifetime Prediction of Mechanical and Structural Components. Ph.D. Thesis, University of Porto, 2014.

[7] Basquin OH. The exponential law of endurance tests. Proc Am Soc Test Mater 1910;10:625–30.

[8] Miner, M.A. (1945). Cumulative damage in fatigue. Transactions of The ASME. Series E. J. Appl. Mech., Vol. 12, pp. 159–164.

[9] Morrow JD. Cyclic plastic strain energy and fatigue of metals. Int Frict Damp Cyclic Plast ASTM STP 1965; 378:45–87.

[10] Ramberg W, Osgood WR. Description of the stress-strain curves by the three parameters. NACA TN-902, National Advisory Committee for Aeronautics, 1943.

[11] Coffin LF. A study of the effects of the cyclic thermal stresses on a ductile metal. Trans ASME 1954;76:931–50.

[12] Manson SS. Behaviour of materials under conditions of thermal stress, NACA TN-2933. National Advisory Committee for Aeronautics; 1954.

[13] Smith RN, Watson P, Topper TH. A stress strain function for the fatigue of metal. J Mater 5:767–78, 1970.

[14] F. Esmaeili, T.N. Chakherlou, M. Zehsaz, Prediction of fatigue life in aircraft double lap bolted joints using several multiaxial fatigue criteria. Materials and Design 59 430–438, 2014.

[15] Gough, H.J., Pollard, H.V., 1935. The strength of metals under combined alternating stress. Proc Inst Mech Engrs 1935;131:3–18.

[16] Gough, H.J., Pollard, H.V., 1937. Properties of some materials for cast crankshafts, with special reference to combined alternating stresses. Proc Inst Automobile Engrs 1937;31:821–93.

[17] Sines, G., 1959. Behaviour of metals under complex stresses. In: Sines G, Waisman JL, editors. Metal fatigue. New York: McGraw-Hill; 1959. p. 145–69.

[18] Findley, W.N., 1959. A theory for the effect of mean stress on fatigue of metals under combined torsion and axial load or bending. J Eng Ind, Trans ASME 1959;81:301–6.

[19] Matake, T., 1977. An explanation on fatigue limit under combined stress. Bull JSME 1977;20:257–63.

[20] McDiarmid, D.L., 1991. A general criterion for high cycle multiaxial fatigue failure. Fatigue Fract Eng Mater Struct 1991;14:429–53.

[21] Papadopoulos, I.V., 2001. Long life fatigue under multiaxial loading. Int J Fatigue 2001;23:839–49.

[22] Wang, Y.Y., Yao, W.X., 2004. Evaluation and comparison of several multiaxial fatigue criteria. International Journal of Fatigue 26 (2004) 17–25.

[23] Findley, W.N., 1956. Theories relating to fatigue of materials under combinations of stress. Colloquium on Fatigue, Stockholm (1955), Springer-Verlag, Berlin, 35.

[24] Findley, W.N., Tracy, J.F., 1973. The Effect of the Intermediate Principal Stress on Triaxial Fatigue of 7075-T6 Aluminum Alloy. Journal of Testing and Evaluation, Volume 1, Issue 5.

[25] Brown, M.W., Miller, K.J., 1973. A theory for fatigue failure under multiaxial stress–strain conditions. Proc Inst Mech Engrs 1973;187:745–55.

[26] Fatemi, A., Socie, D.F., 1988. A critical plane to multiaxial fatigue damage including out-of-phase loading. Fatigue Fract Eng Mater Struct 1988;11(3):149–65.

[27] Socie, D.F., 1987. Multiaxial fatigue damage models. J Eng Mater Tech 1987;109:293–8.

[28] Chu, C.C., Conle, F.A., Bonnen, J.J., 1993. Multiaxial stress–strain modeling and fatigue life prediction of SAE axle shafts. In: McDowell DL, Ellis R, editors. Advances in multiaxial fatigue, ASTM STP 1191. Philadelphia: ASTM; p. 37–54.

[29] Liu, K.C.,1993. A method based on virtual strain-energy parameters for multiaxial fatigue life prediction. In: McDowell DL, Ellis R, editors. Advances in multiaxial fatigue, ASTM STP 1191. Philadelphia: ASTM; p. 37–54.

[30] Glinka, G., Plumtree, A., Shen, G., 1995. A multiaxial fatigue strain energy parameter related to the critical plane. Fatigue Fract Eng Mater Struct;18(1):37–46.

[31] Ellyin, F., 1997. Fatigue damage, crack growth and life prediction. Chapman & Hall.

[32] Jahed, H., Varvani-Farahani, A., Upper and lower fatigue life limits model using energy-based fatigue properties, International Journal of Fatigue, 28 (2006) 467-473.

[33] CEN (2005c) 1993-1-9:2005, Eurocode 3 - Design of steel structure - Part 1-9: Fatigue, European Committee for standardization, Brussels.

[34] Paris, P.C., Erdogan, F., 1963. A critical analysis of crack propaga-tion laws. Transactions of the ASME Series E: Journal Basic Engineering, Vol. 85, pp.528–34.

[35] Tanaka, K., 1974. Fatigue crack propagation from a crack inclined to the cuclic tensile axis. Engineering Fracture Mechanics; 6:493-507.

[36] Socie, D.F., Marquis, G.B., 2000. Multiaxial fatigue. USA: SAE International. ISBN 0 7680 0453 5.

[37] Lebaillif, D., Rechob, N., 2007. Brittle and ductile crack propagation using automatic finite element crack box technique. Engineering Fracture Mechanics, Volume 74, Issue 11, Pages 1810–1824.

[38] Da Silva, A.L.L., 2015. Advanced methodologies for the fatigue analysis of representative details of metallic bridges. Ph.D. Thesis, University of Porto, Portugal.

[39] Correia, J.A.F.O., De Jesus, A.M.P., Tavares, S.M.O., Moreira, P.M.G.P., Tavares, P.J.S., Calçada, R.A.B., 2016. Mixed-mode fatigue crack propagation rates of currents structural steels applied for bridges and towers construction. Bridge Maintenance, Safety and Management (IABMAS'16), Foz do Iguaçu, Brazil, 26-30 June 2016.

[40] Öztürk, F., Correia, J.A.F.O., Rebelo, C., De Jesus, A.M.P., Simões da Silva, L., (2016). Fatigue assessment of steel half-pipes bolted connections using local approaches. Structural Integrity Procedia (XV Portuguese Conference on Fracture), in press.

[41] De Jesus, A.M.P., Matos, R., Fontoura, B.F.C., Rebelo, C., Simões da Silva, L., Veljkovic, M., 2012. A comparison of the fatigue behavior between S355 and S690 steel grades, Journal of Constructional Steel Research, Volume 79, December 2012, Pages 140–150.

[42] Correia, J.A.F.O., De Jesus, A.M.P., Fernández-Canteli, A., Calçada, R.A.B., 2015. Modelling probabilistic fatigue crack propagation rates for a mild structural steel, Frattura

ed Integrita Strutturale, ISSN 1971-8993, Vol. 31, 2015, 80-96.

[43] ASTM – American Society for Testing and Materials. ASTM E606-92: standard practice for strain controlled fatigue testing. In: Annual book of ASTM standards, part 10; 1998. p. 557–71.

[44] ASTM – American Society for Testing and Materials. ASTM E647: standard test method for measurement of fatigue crack growth rates. In: Annual book of ASTM standards, vol. 03.01. West Conshohocken, PA: ASTM – American Society for Testing and Materials; 2000. p. 591–630.

[45] Abaqus analysis user's manual version 6.10. Dassault Syst_emes Simulia Corp.: Providence, RI, USA.

[46] CEN (2005b) 1993-1-8:2005, "Eurocode 3 - Design of steel structures - Part 1-8: Design of joints ", European Committee for Standardization, Brussels.

[47] Guilherme Gandolfi Figueiredo, Structural behavior of hybrid lattice – tubular steel wind tower, 2013.